

NOVEL SULFUR SURFACE PASSIVATION FOR N- AND P-TYPE SILICON

by

Robert Theisen

A thesis submitted to the Faculty of the University of Delaware in partial fulfillment of the requirements for the degree of Master of Science in Material Science and Engineering

Fall 2020

Copyright 2020 Robert Theisen
All rights reserved

NOVEL SULFUR SURFACE PASSIVATION FOR N- AND P-TYPE SILICON

by

Robert Theisen

Approved:

William N. Shafarman, Ph.D.
Professor in charge of thesis on behalf of the Advisory Committee

Approved:

Darrin J. Pochan, Ph.D.
Chair of the Department of Materials Science and Engineering

Approved:

Levi T. Thompson, Ph.D.
Dean of the College of Engineering

Approved:

Louis F. Rossi, Ph.D.
Vice Provost for Graduate and Professional Education and Dean of the
Graduate College

ACKNOWLEDGMENTS

William N. Shafarman, Ph.D and Ujjwal Das, Ph.D for their patience, support, and chances to expand my knowledge throughout my graduate experience.

The Georgia Institute of Technology and the University of Nevada. I never would have gotten the chance to work on this project if these institutions were not working on this project alongside the IEC.

Isaac Lam, Steve Hegedus, Kevin Dobson, Anish Soman, Greg Hanket, and the rest of the IEC for answering my questions and helping me along during my first days at the Institute of Energy Conversion

This research is based upon work supported by the U.S. Department of Energy's Office of Energy Efficiency and Renewable Energy (EERE) under the Solar Energy Technology Office (SETO), Award Number DE-EE0008554.

Disclaimer: "This report was prepared as an account of work sponsored by an agency of the United States Government. Neither the United States Government nor any agency thereof, nor any of their employees, makes any warranty, express or implied, or assumes any legal liability or responsibility for the accuracy, completeness, or usefulness of any information, apparatus, product, or process disclosed, or represents that its use would not infringe privately owned rights. Reference herein to any specific commercial product, process, or service by trade name, trademark, manufacturer, or otherwise does not necessarily constitute or imply its endorsement, recommendation, or favoring by the United States Government or any agency thereof. The views and opinions of authors expressed herein do not necessarily state or reflect those of the United States Government or any agency thereof.

This thesis is dedicated to my mother Deborah, my father Timothy, and my sister

Kathryn

TABLE OF CONTENTS

LIST OF TABLES	vi
LIST OF FIGURES	vii
ABSTRACT.....	ix
Chapter	
1 BACKGROUND and MOTIVATION	1
2 TECHNICAL BACKGROUND.....	5
3 EXPERIMENTAL.....	16
3.1 Wafer Selection and Cleaning	16
3.2 Quinhydrone-Methanol (QH) Passivation	17
3.3 Custom-built Sulfurization/Selenization System.....	18
3.4 Quasi-Steady State Lifetime Measurement	20
3.5 Sheet Resistance.....	24
3.6 SRH Formalism: Modelling of D_{it} and Q_f	25
4 RESULTS	26
4.1 Outline of Experiments.....	26
4.2 Final Results	31
4.2.1 QH Confirmation of Wafer Cleaning	31
4.2.2 Surface Passivation by H_2S Reaction at Different Temperatures	32
4.2.3 Reaction Time and SRV Stability.....	35
4.2.4 S Concentration, Flow Rate	38
4.2.5 Se Passivation and S/Se Mixtures.....	40
4.2.6 Diffused Wafer Passivation	41
4.2.7 Lifetime Modelling for D_{it} and Q_f	48
5 CONCLUSION.....	53
BIBLIOGRAPHY.....	55

LIST OF TABLES

Table 3.1 Characteristics of wafers provided by GIT. Thickness is calculated from their weight and area, sheet resistance is measured by 4-probe method, resistivity and dopant levels are calculated.....	17
Table 4.1: Experimental design for concentration and gas flow.	28
Table 4.2: Surface cleaning and passivation steps studied for n ⁺ and p ⁺ diffused n-type Cz Si wafers.....	30
Table 4.3: Analyzed samples for modelling of D _{it} and Q _f	30
Table 4.4: Effective minority carrier lifetime (τ_{eff}) at excess carrier density of $1 \times 10^{15} \text{ cm}^{-3}$ for SP-n, GT-n and GT-p wafers with and without the HNA steps. The values are averaged over 3 wafers for each type.....	32
Table 4.5: Surface Passivation quality of sulfur passivation results as compared to Al ₂ O ₃ (ALD) and thermal oxide passivation.....	39
Table 4.6: Dopant-diffused wafers used for sulfur passivation. J ₀ and implied VOC were estimated from QSSPC before S/Se process.....	42
Table 4.7: J ₀ values of Si dopant-diffused n-n ⁺ wafers passivated at 550°C by 3.5% H ₂ S.	47
Table 4.8: Extracted D _{it} and Q _f from lifetime modelling.....	51

LIST OF FIGURES

Figure 2.1: Typical IV curve of a solar cell.[3]	5
Figure 2.2: Diagram of chemical surface passivation. Bond termination at the surface removes defect levels and decreases recombination rate. ([10])	9
Figure 2.3: Diagram of charge-based passivation. Fixed charges in the passivation layer create a local electric field and drive away the minority carrier, reducing its concentration and improving recombination rate. ([10]).....	10
Figure 2.4: Diagram of a basic solar cell. [20]	14
Figure 3.1: Picture of sulfurization/selenization system.....	19
Figure 3.2: Typical time-temperature profile for 60 min reaction at 550°C.....	20
Figure 3.3: Suns-photoconductance curve (top) is interpreted into lifetime/carrier density curve (bottom)	22
Figure 3.4: The structure of a dopant Si wafer as pertaining to a 4-point resistance measurement. The current travels in parallel in both regions.....	24
Figure 4.1 Example fitting using a program made by Brent Shu [8].....	31
Figure 4.2 Temperature optimization for H ₂ S passivation at 3.4% in Ar concentration ...	33
Figure 4.3: Initial degradation study of GT-n, GT-p, and SP-n wafers	34
Figure 4.4: Relationship between τ_{fit} and τ_{eff} . Clear averages for τ_{fit} are shown for each type of wafer, and estimates τ_{bulk}	34
Figure 4.5 (Top, a) Lifetime as a function of reaction length for n-type and p-type textured Cz Si wafers. (Bottom, b) Degradation of lifetime of S passivated GT-n and GT-p wafers show slower degradation rate for longer reaction time irrespective of wafer types and surfaces	36
Figure 4.6: Long-term stability of a-SiN _x capping layer with/without H ₂ S passivation. Periods after day 90 are post-firing, according to Figure 4.7.	37

Figure 4.7: Sample temperature curve for GIT firing process (from GIT).....	37
Figure 4.8: Gas flow and concentration in H ₂ S passivation. A green filled data point is at double flow rate, and a purple filled data point is at half flow rate	38
Figure 4.9: (Top) SRV as a function of reaction temperature at 0.32% in Ar (Bottom) SRV as a function of H ₂ Se concentration in an H ₂ Se/H ₂ S gas mixture	41
Figure 4.10: n-p ⁺ (Top) and n-n ⁺ (Bottom) S surface passivation with different cleaning and passivation processes.	43
Figure 4.11: Stability of S passivation with/without a-SiN _x capping layer on dopant-diffused Si wafers. HF-60 cleaning/reaction process used to make this graph.	45
Figure 4.12: Relationship between J ₀ and R _{sheet} on n-n ⁺ Si wafers.....	48
Figure 4.13 Estimated D _{it} values as a function of reaction temperature (top) and decay time (bottom).	50
Figure 4.14 Relationship between D _{it} and Q _f	52

ABSTRACT

The reduction of recombination at the surface of a silicon wafer is an important factor in improving the efficiency of solar cells. Thermal oxidation is the most common method for Si surface passivation and has excellent performance, but the high temperature process can degrade the bulk quality of silicon, which adversely affects solar cell performance. Deposition of a thin aluminum oxide layer is another common passivation method that works well on p-type silicon thanks to its high negative fixed charge that repels electron minority carriers away from the surface and it is very stable under light, but this same aspect makes it worse on n-type silicon for hole minority carriers. The objective of this research is this to create a lower temperature passivation layer than the thermal SiO₂ that can withstand an industry-standard screen-printed metallization process, while being applicable to both types of surfaces unlike Al₂O₃. Sulfur and selenium are proposed theoretically to be good candidates for this purpose because of their ability to cap multiple surface bonds at once, as well as their similar bond angles and lengths to Si. [1] Experimental work done by S. Liu et al. [2] at IEC has demonstrated a lifetime >2000 μs and an Surface Recombination Velocity (SRV) < 3 μs by H₂S gas phase reaction, which can match thermal SiO₂. This thesis will expand upon that work, offer some explanations of passivation mechanism and apply the process to passivate dopant-diffused Si surface.

A custom-built sulfurization/selenization reactor is used for the passivation of HF-cleaned n- and p-type silicon wafers with and without a diffused n⁺ or p⁺ emitter. The

samples were reacted in H₂S and H₂Se for S and Se passivation, respectively, with a background Ar gas flow for dilution. Reactions were performed at a range of temperatures between 400-650°C, and with reaction times between 15 to 210 minutes. The best lifetimes and SRVs are achieved at 550°C (>2000 μs, < 3 cm/s, similar to previous work, ([2]) with reaction duration not having a significant effect on as-passivated lifetime. S passivation decays rapidly in air, decaying by an order of magnitude within half an hour. A longer reaction time (≥ 60 min) can reduce the rate at which the S passivation decays in air, though further processing is needed to fully stabilize the passivation. A deposited a-SiN_x layer on top of the S layer prevents degradation for some months. Some attempts have been made at Se and S/Se mixture passivation, but current results suggest that Se passivation is inferior compared to S passivation. In terms of how the passivating gas interacts with the Si surface, a higher net Ar flow clearly improves the performance of the S passivation, while there is a certain minimum concentration of H₂S for significant passivation to occur. Dopant diffused n-n⁺ and n-p⁺ wafers follow a similar passivation model to the undiffused n and p-type Si wafers.

Modelling of the lifetime data to estimate surface state density (D_{it}) and fixed charge density (Q_f) suggests that higher lifetime is related to a lower D_{it} , but a linear relationship between D_{it} and Q_f is present and unexplained. In order to fully understand the S passivation mechanism, further studies, including capacitance-voltage (CV) testing, are necessary to precisely determine D_{it} and Q_f and confirm modelling trends.

Chapter 1

BACKGROUND AND MOTIVATION

Solar energy has been a promising avenue to replace fossil fuels ever since the 1950s, when the first photovoltaic solar cell was demonstrated using silicon by Bell Labs. [3] This was done by creating a p-n junction within a wafer of Si using dopants. Today, solar power only produces a small fraction of the world's electricity, about 3% of US total generation as of 2019, [4] but its use is accelerating, with ~40% of added electricity generation in 2019 from solar. [4] At its most basic level, a solar cell is made by doping a semiconductor (commonly silicon) such that a junction is formed between an n-doped region and a p-doped region. [5] The presence of this junction forms an electric field, which separates the electrons and holes and drives excited carriers towards an external load, where the charge is extracted. The carriers then recombine with their opposite charges, completing the circuit and generating current.

The performance of a solar cell is defined by its efficiency, which is the fraction of energy in the incident light that gets converted into usable energy. Efficiency is impacted by several different conditions, including how many carriers are generated from the incident light, the strength of the p-n junction, and how well these electrons can be collected in the contacts. Contact design is related to collection of photogenerated carriers and letting incident light into the cell, while separating and generating carriers is closely related to keeping recombination low. Recombination is where an excited electron comes

down from a higher energy band into a hole position, releasing energy. This doesn't have to be the same hole that the electron left when it was originally excited. There doesn't have to be light for recombination to occur, as there is a certain amount of recombination brought on by the pn junction itself. This process releases energy as light or heat and can waste a significant amount of power that the cell would otherwise generate. There are a few particularly important parameters that quantitatively describe recombination within a solar cell: minority carrier lifetime, and surface recombination velocity (SRV). Lifetime is the duration of time a minority carrier is expected to last before recombining, where a higher lifetime means that recombination is happening at a slower rate. In solar cells, surfaces can be particularly suited to recombination, as the truncated lattice provides ample defect sites for Shockley-Read-Hall (SRH) recombination. [5] SRV is an abstract measurement of how fast carriers diffuse towards the surface to recombine. If this value were infinite, carriers would move towards the surface at the maximum physically achievable rate (typically $\sim 10^7$ cm/s) possible, while an SRV of zero would mean no carriers move towards the surface. By reducing the rate at which carriers move, the less will make it to the surface sites where recombination is easier. Thus, one way in which solar cell performance can be improved is reducing SRV. This can be achieved by reducing the number of dangling bonds at the surface, which is a purpose of passivation. The best Si solar cells reach $SRV = 1-10$ cm/s.

Passivation, in its most general sense, encompasses approaches to make the surface of a material more "passive", i.e. reducing recombination at the surface or junction. There are two major approaches to passivation, with materials prioritizing one

method over the other. The first approach is the termination of defects, especially dangling bonds on the surface of the silicon wafer, known as chemical surface passivation. The other common approach to passivation is to deposit a layer of material that would have a significant fixed charge of the same sign with the topmost layer, known as field effect passivation. This creates an electric field that drives carriers away from the surface, thus reducing recombination by reducing the number of available one type of carriers. Some downsides of current passivation materials include temperature concerns; too high for thermal oxide (SiO_2) affects bulk quality and thermal instability of low temperature deposited amorphous Si (a-Si:H) limits downstream cell processing temperature. Some passivation materials work better on certain doping types, such as Al_2O_3 , which works better on p-type silicon due to its high negative fixed charge density and not as well on n-type silicon. These will be discussed in more detail in the next section.

When all of this is considered, there is a considerable interest to develop a low temperature surface passivation process that can match the performance of thermal SiO_2 , stable under industry-standard metallization schemes and performs equally well on both n- and p-type silicon. Al_2O_3 could fit this description to some extent, but its fixed charge prevents it from being applicable on both types of surfaces. Thus, the objective of this project is to find a material that can meet these qualifications, and the approach is to use the chalcogens sulfur and selenium that have a favorable chemical/bonding structure that could increase their applicability. First proposed by Kaxiras, the valence state of S and Se is suited to capping multiple bonds on a (100) silicon surface and creating a crystal

structure that is very similar to Si, thus minimizing stress. [1] Further research was performed by Ali and Tao, who passivated Si (100) with a mixture of ammonium hydroxide and ammonium sulfide, where the reduction of surface states was postulated by studying the formation of Schottky barrier contacts on n- and p-type Si wafers with and without S passivation. [6] The wafers with passivation showed a greater sensitivity to the metal work function, thus being closer to the ideal theory. [6] Recently, lifetime and SRV data has been reported on n- and p-type Cz Si wafers via reaction with H₂S, [2] and exhibited lifetime and SRV values similar to a-Si:H passivation. [7]

This thesis will expand the scope of knowledge related to S and Se passivation and identify the critical components to maximizing the performance and usability of such. Section 2 will consist of the needed technical background to understand the rest of the thesis and explain how this knowledge will be built upon. Section 3 will consist of the outline of experimental tools and procedures that were used to collect the data for this thesis. Section 4 will explain the precise experiments performed and the results of said experiments in detail. Finally, Section 5 will be a short conclusion of the results and suggestions for further work.

Chapter 2

TECHNICAL BACKGROUND

This section will begin with a brief review of current (I) – voltage (V) curves of a solar cell. The creation of a IV curve is the primary way the performance of a solar cell is measured, and involves varying the voltage bias on the cell over a range of values, and measuring the current I (or current density J) that passes through the cell as a function of said bias. From this measurement, a graph like Figure 2.1 would be made that is described by Equation 2.1, and important parameters can be retrieved from it.

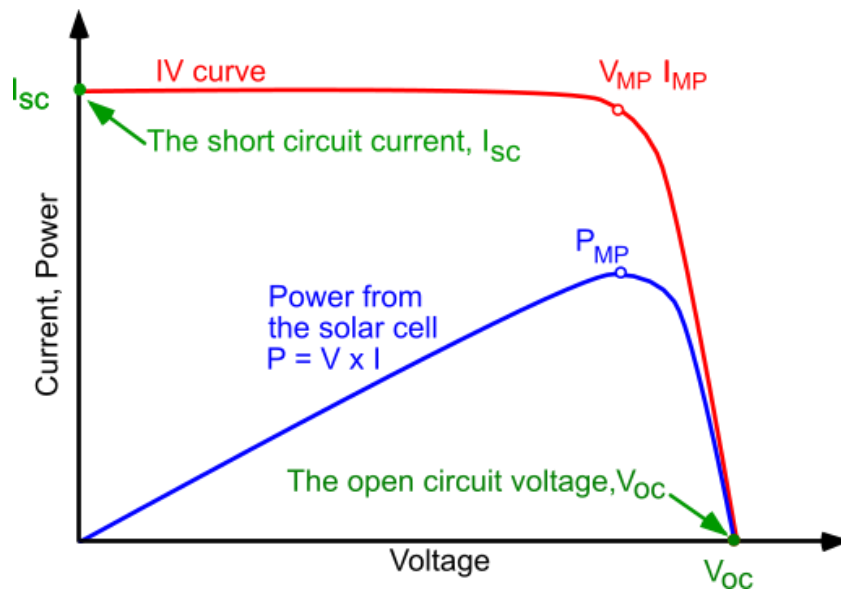


Figure 2.1: Typical IV curve of a solar cell. [5]

$$I = I_L - I_0 \left[\exp\left(\frac{qV}{nkT}\right) - 1 \right] \quad (2.1)$$

Equation 2.1 describes the measured current as a combination of two sources: The current from incident light (I_L) and the current generated by the applied voltage. The second part is composed of the darklight saturation current (I_0) and a number of fundamental terms: the charge of an electron (q), the voltage bias through the cell (V), an ideality factor (n), the Boltzmann constant (k), and the temperature in °C (T). The short circuit current (I_{SC}) is the current generated by the light when there is no bias brought by an induced voltage. The open circuit voltage (V_{OC}) is the applied voltage at which no net current is generated, and is closely related to recombination. There is no net flow of carriers at this state. P_{MP} on the graph above is the maximum amount of power (current $I \times$ voltage V) that can be extracted from the solar cell. The power conversion efficiency (η) and the fill factor (FF) of the solar cell are defined by Equation 2.2. $100\text{mW}/\text{cm}^2$ is a standard solar irradiance value that can vary based on many conditions.

$$FF = \frac{P_{MP}}{V_{OC} * I_{SC}}; \eta = \frac{V_{OC} I_{SC} FF}{P_{in}}; P_{in} = \frac{100\text{mW}}{\text{cm}^2} * A \quad (2.2)$$

This calculation of current makes a few assumptions with regard to series and shunt resistances. First, it assumes that series resistance (resistance from interfaces with the contact or from emitter to base) does not impact the solar cell. If series resistance (R_{series}) is present, this changes the qV term in Equation 2.1 to $q(V + IR_{series})$. This does not affect open circuit voltage, but does impact the slope of the IV curve at V_{OC} and can reduce I_{SC} . Equation 2.1 also assumes that shunt resistance (R_{shunt}) is infinite. When shunt resistance is not infinite, defects in the cell create an alternate path through the bulk,

adding the additional term $-V/R_{\text{shunt}}$ to the right side of Equation 2.1. This does not impact I_{SC} , but does lower V_{OC} . Taking these assumptions into account, P_{MP} is highest when V_{OC} and I_{SC} , and the fill factor FF are at their highest, and V_{OC} can especially be increased by reducing recombination at the surface. Reducing recombination at the surface is the primary point of passivation, and the bulk of this project.

There are two primary approaches to the passivation of a surface: chemical surface passivation, and field effect passivation. These can be understood by considering the equation for SRH recombination in the context of recombination at a surface. [8] SRH recombination is the recombining of excited electrons and holes via a trap state that resides in the forbidden zone of the band diagram. These traps are created by defects within the crystal lattice, e.g. vacancies, interstitials, extrinsic defects, and so on. The carriers trapped in energy levels that are closest to the center of the forbidden gap are harder to escape than in the energy levels closer to a band, thus mid-gap defect levels act as efficient SRH recombination centers. The truncated lattice of a surface has many defect levels for SRH recombination. The standard equation for SRH recombination rate (U_T) for a given concentration of carriers n and p is shown in equation 2.3 where n_1 and p_1 are intrinsic concentrations based upon a number of recombination factors, including the concentration of carriers N_C and energy of the trapping level E_t , and τ_{h0} and τ_{e0} , which are the lifetimes of holes and electrons, respectively. [9]

$$U_T = \frac{np - n_i^2}{\tau_{h0}(n + n_1) + \tau_{e0}(p + p_1)}, n_1 = N_C \exp\left(\frac{E_t - E_c}{kT}\right); n_1 p_1 = n_i^2 \quad (2.3)$$

Reinterpreting the hole and electron lifetimes in the context of surface recombination gives the following equation for recombination rate at the surface (U_s): [10]

$$U_s = \frac{(n_s p_s - n_i^2) v_{th} N_{st}}{\frac{n_s + n_1}{\sigma_p} + \frac{p_s + p_1}{\sigma_n}} \quad (2.4)$$

Here n_s and p_s are the electron and hole concentration at the surface, v_{th} is thermal velocity (increases with T), N_{st} is the number of interface trap states, and $\sigma_{n,p}$ are the capture cross sections (a measurement of the area an electron must cross to be captured from the conduction band). Thermal velocity and capture cross section are both functions of temperature, which is impractical to control in normal solar cell operation. n_1 and p_1 are functions of the trap levels, which are not controllable. Thus, the approaches of reducing U_s are to reduce the number of surface states (N_{st}), or reduce the concentration of the minority carriers at the surface (n_s, p_s). It is important to keep in mind that recombination doesn't always happen at the surface and can happen in the bulk. Some defect passivating elements can diffuse into the bulk to contribute to this. [11]

The primary pathway to reduction of surface states is to fill the dangling bonds created by the truncated lattice on the surface of the silicon, thus decreasing the number of trap states and reducing the rate of recombination. This approach to chemical surface passivation will use an element with a valence electron structure that can bind to Si without any free radicals left over and create as little stress and strain as possible from bonding to the Si. Two elements in particular meet these criteria and have been used for decades in the passivation of solar cells: oxygen and hydrogen. These elements are created on the surface via oxidation and hydrogenation, respectively, as shown in figure 2.2. The reduction in surface states can be characterized by the measurement of surface state density (D_{it}), which is the the concentration of trap states at the surface of the wafer.

D_{it} can replace the interface trap density N_{st} in equation 4 by integrating over the entire band gap (equation shown in section 4.2.6), and can be experimentally measured by creating a metal-insulator-semiconductor (MOS) [12] structure, measuring capacitance voltage (CV) and conductance voltage (GV) curves from the structure, and comparing them to ideal curves on pure Si.

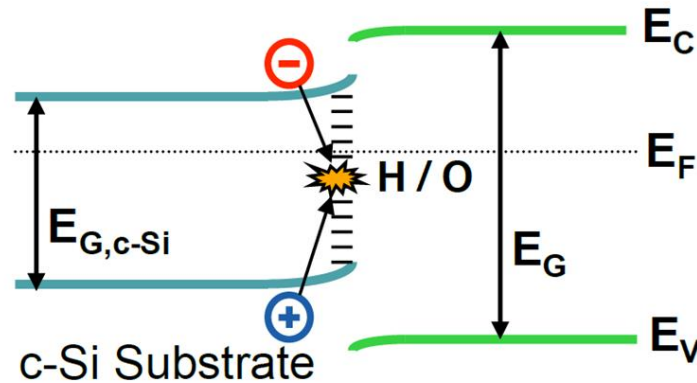


Figure 2.2: Diagram of chemical surface passivation. Bond termination at the surface removes defect levels and decreases recombination rate. ([10])

To reduce n_s or p_s , an electric field in addition to the electric field generated by the cell junction is used to drive one carrier type away from the surface. This is the core theory behind field-effect passivation. For this purpose, there are a few different techniques. The first is the surface doping of the silicon wafer. While performance can differ, the general effect can be achieved via inserting phosphorus atoms for an n^+ layer [13] or boron for a p^+ layer. [14],[15] This is an important part of how junctions are formed within a solar cell and is referred to as a front surface field (FSF) or a back surface field (BSF) depending on where it is in the wafer. An alternate way of achieving

this is to place a passivation layer on top of the silicon surface with a like fixed charge to repel carriers. [16] A fixed charge within a passivation material is the result of interactions with the bulk silicon. For example, an Aluminum Oxide (Al_2O_3) layer deposited on Si has a negative fixed charge, where there are a number of ionic charges within the Al_2O_3 as a result of defects, such as interstitial H or Al vacancies. This creates an electric field at the interface, driving electrons away from the surface of the wafer as illustrated in Figure 2.3. Similarly, a-SiN_x:H has a positive fixed charge, which repels holes away from the surface. The amount of fixed charge per unit area is the fixed charge density (Q_f), and it can be experimentally determined from the same CV and GV tests as D_{it} .

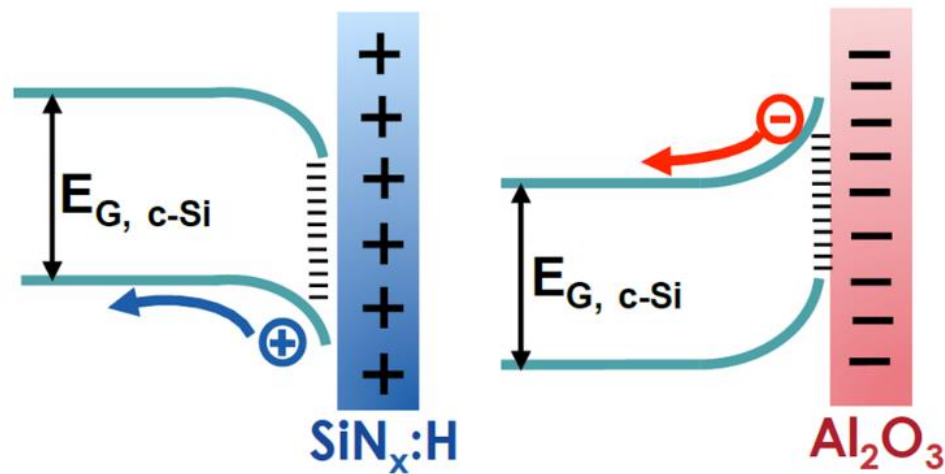


Figure 2.3: Diagram of charge-based passivation. Fixed charges in the passivation layer create a local electric field and drive away the minority carrier, reducing its concentration and improving recombination rate. ([10])

Thermally grown silicon dioxide (SiO_2) is the most common chemical passivation method with 25% solar efficiency (i.e. can convert 25% of the energy from sunlight into

usable energy via photovoltaics) and SRV as low as 0.5 cm/s after a full annealing process for the addition of contacts. [17] The process is not deposition, but instead oxidation of the silicon surface at a high temperature, usually over 900°C. [18] This process works well at many different levels of doping, since it doesn't have a significant field effect. However, there are still areas in which thermal oxidation falters, most notably significant complications from impurities for high temperature processing, instability under UV light, and comparatively poor results for p-type Si. [11] To avoid some of these downsides, low temperature processes have been pursued, like PECVD and ALD [19],[20] to form passivation layers that are often very thin (a few nm).

Amorphous silicon nitride ($a\text{-SiN}_x$) is a very stable material for silicon passivation. [21] It is grown by plasma enhanced chemical vapor deposition (PECVD), which is typically done at $T \approx 400\text{C}$. [21] J_0 and SRV values are acceptable, with the best $J_0 \sim 100 \text{ fA/cm}^2$ and the best SRV as low as 1.7 cm/s. [11] $a\text{-SiN}_x$ has a large positive fixed charge density (around 10^{12} cm^{-2}), and thus works best on n-type wafers. It also has several other benefits: its refractive index can be tuned over a large range (1.9-2.9) to also act as an anti-reflection coating, [22] and the passivation process contains a lot of hydrogen, which can passivate the bulk. [23] Essentially, $a\text{-SiN}_x$ can passivate with both chemical and field-effect mechanisms. It is also a core component of oxide-nitride stacks, where an SiO_2 layer is "capped" with an $a\text{-SiN}_x$ layer that chemically stabilizes the oxide layer while giving all the benefits of $a\text{-SiN}_x$ passivation. [11]

Al_2O_3 is the primary material for field-effect passivation. Al_2O_3 passivation on Si has a substantial negative fixed charge density ($10^{12}\text{-}10^{13} \text{ cm}^{-2}$), which makes it suitable

for deposition on Si wafers doped with p^+ layers. [24] Al_2O_3 is also particularly stable by itself. [25] The Al_2O_3 is usually deposited by the ALD technique, which is a much more controlled technique compared to PECVD with respect to thickness and uniformity. [26]. However, ALD deposition is very slow (<0.5 nm/min for a passivation layer of > 10 nm), which limits how many cells can be manufactured. PECVD can be used to deposit Al_2O_3 at a much faster rate than ALD, but doesn't get the best quality. [11]

Hydrogenated amorphous silicon (a-Si:H) is a passivation approach using PECVD deposition at $T \approx 200-250^\circ C$. [2] This amorphous silicon can be layered with crystalline Si to create efficient solar cell structures. [27],[28] The a-Si:H/c-Si interface has a large energy step in both the conductance and valence bands, thus provides a field-effect style passivation for both n and p-type c-Si, while the hydrogen (within the a-Si:H) is the source of the chemical passivation effect. There is a significant correlation between H concentration and passivation quality. [11] The best a-Si:H passivation results have an SRV below 3 cm/s. [29] Deposition at a low temperature is a major cost reduction factor by itself, but a-Si:H passivation may degrade under sustained illumination from the breaking of weak Si-Si bonds, [30] and the layer itself cannot withstand downstream process temperatures above $300^\circ C$. [31]

An example solar cell is shown in Figure 2.4, and is the end result of a series of processing steps to create an n-p junction within the silicon wafer and attach suitable contacts. [21] The example shown here is from a boron-doped p-type Si wafer. The first step in manufacturing of an Si solar cell is the cutting of a single crystal from a cast silicon block. This is done using diamond wire saw, with typical thickness around 180

μm . The manufacturing of the cell itself starts with the chemical etching and texturing of the silicon surface via chemical baths. Etching in KOH, for example, creates a textured surface with square pyramids aligned to (111) planes. After the surface is etched, the wafer is then cleaned. This usually involves the oxidation of the surface to remove impurities, then H-termination to prepare for future steps, like doping. After cleaning, the emitter is created by the diffusion of phosphorous into the p-type bulk, creating an n^+ layer near the top of the wafer. This n^+ -p junction separates electrons and holes by electric field. High concentrations of phosphorous also help with reducing resistance between the Si and the contact. [21] Next, the wafer is covered with an anti-reflection coating to reduce the amount of light that bounces off the wafer surface to allow more light absorbed in the Si. As previously mentioned, $a\text{-SiN}_x$ is a common anti-reflection coating that also doubles as a passivation material, so it is especially useful here. The front side is then finalized by the application of the contacts. In this example, it is done by screen-printing of metal “fingers” across the top of the wafer. The thickness of these fingers is optimized to minimize the amount of area covered while minimizing resistive losses. At the same time, an Al layer is screen-printed onto the back of the wafer. This serves as the back contact for the wafer, and also creates the hole contact by Al doping as the wafer cools down.

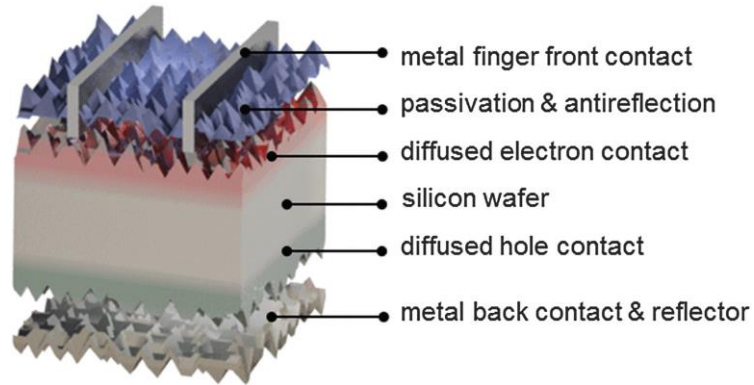


Figure 2.4: Diagram of a basic solar cell. [21]

In summary, chemical passivation is desirable if a material can bond with multiple sites on Si, create a similar molecular structure, and can remain stable under exposure to air, while field-effect passivation is preferred when the passivation material matches the charge of the surface. SiO_2 gives the best lifetime and J_0 values, a-SiN_x can be deposited at lower temperatures and can act as an anti-reflective coating, Al_2O_3 is suited for passivating p-type and p^+ doped Si, while a-Si:H can be used for passivation at temperatures below 250°C . It is important to remember that most passivation materials can incorporate both methods of reducing n_s and p_s , even if the material favors one method over the other. For this project chemical surface passivation is preferred, as to maximize the flexibility and applicability of the passivation layer. A number of group V and VI elements fit this description, including sulfur [32] and selenium, as discussed previously. As for the chemical reaction, H_2S has been the primary passivation gas for reaction with Si. [2] H_2S can react with S to form SiS_2 to fill Si dangling bonds [33] and prevent unwanted surface recombination loss. [6] It has previously been proven that S can achieve SRV values below 3 cm/s via this method, and Liu et al have worked

extensively on this subject. [34] Primary results include a lifetime $> 2000 \mu\text{s}$ on n-type silicon at an H_2S reaction temperature of 550°C , preliminary exploration of reaction chemistry via XPS, and an investigation into the stability of the resultant passivation layer in air. [2]

Chapter 3

EXPERIMENTAL

3.1 Wafer Selection and Cleaning

This project will use Si wafers provided by the Georgia Institute of Technology (GIT). GIT has prepared planar and textured p- and n-type 6" pseudo-square wafers in a series of wet chemical etching and cleaning processes. As a first step, the wafers have gone through a damage etch removal in potassium hydroxide (KOH) solution to remove ~ 15 μm of Si from each side. This is followed by a series of surface cleaning steps to remove any residual impurities using hydrofluoric acid (HF) – sulfuric acid (H_2SO_4) – HF – hydrochloric acid (HCl) – HF steps with a deionized (DI) water rinse in between each step. [35] Once received from GIT, these wafers are cut into 1"x1" squares via laser, and further cleaning is performed at IEC to remove debris from this process. The typical cleaning process is as follows, [2]

- 10% HF for 1 min : remove residual oxides on the surface of the wafer, and form an H-terminated surface
- 1 min Si etching in a mixture of (1:100) HF and nitric acid (HNO_3) (HNA etch): isotropic etching for a consistent wafer surface and removes any laser debris
- 5 mins Piranha oxidation (mixture of $\text{H}_2\text{SO}_4 - \text{H}_2\text{O}_2$) : remove organic residue by two different processes: dehydration (removal of the H-terminated surface from

the first HF step) and oxidation (to prepare the surface for the next step of the cleaning process)

- 10% HF : remove the oxides from the previous step and terminate with H.

Each step listed here has a DI water rinse in-between. Once this cleaning is completed, the samples are immediately loaded into the sulfurization chamber for passivation.

Textured dopant-diffused n-n⁺ and n-p⁺ wafers have also been provided. These are n-type wafers symmetrically diffused on both surfaces by additional phosphorous/boron doped layer to achieve n-n⁺ and n-p⁺, respectively. The cleaning process for this series of wafers would have to be altered, as too much HNA etching can remove the thin dopant diffused layer. This was the subject of experimentation at IEC, and the results are listed in section 4. A full summary of the wafer properties are listed below in table 3.1

Table 3.1 Characteristics of wafers provided by GIT. Thickness is calculated from their weight and area, sheet resistance is measured by 4-probe method, resistivity and dopant levels are calculated.

Wafer Type	Sheet Resistance (Ω)	Thickness (cm)	Resistivity ($\Omega.cm$)	Dopant Level ($10^{15} cm^{-3}$)
GT-n	151	0.016	2.4	1.9
GT-p	107	0.016	1.7	8.4
n-n+	51	0.019	---	---
n-p+	238	0.019	---	---

3.2 Quinhydrone-Methanol (QH) Passivation to test surface cleanliness

A passivation method in quinhydrone methanol [36] solution was used to confirm surface cleanliness as well as serve as a comparison point for future cleaning

optimization. A liquid solution is prepared with 0.43 g of quinhydrone mixed in 100 ml MEOH, then split into two plastic ziplock bags. The cleaned Si wafer can be placed into one of these solutions and can be analyzed for lifetime while the sample is still within the solution bag. This is necessary because the QH passivation degrades rapidly outside of the bag. [36] Quinhydrone passivation is often used to measure the bulk lifetime of the wafer, as the recombination velocity at the surface is very low (< 5 cm/s).

3.3 Custom-built Sulfurization/Selenization system

For this project, a custom-built sulfurization and selenization system made by the IEC was used to react cleaned wafers. [2] A picture of the reactor is provided in Figure 3.1. There are two reaction chambers, SR1 and SR2. SR1 is a removable tube that can accommodate 3 1"x1" wafers per reaction, and uses a separate heating jacket to increase temperature. The heating jacket can be heated up to 700°C at a ramping rate of 40°C/min. Ar and H₂S gases are provided without dilution. The argon gas is pure to a 6N purity level, while the H₂S gas is largely pure, with a < 500 ppm H₂O impurity. H₂Se is diluted in Ar (14% in Ar) because of H₂Se's toxicity.

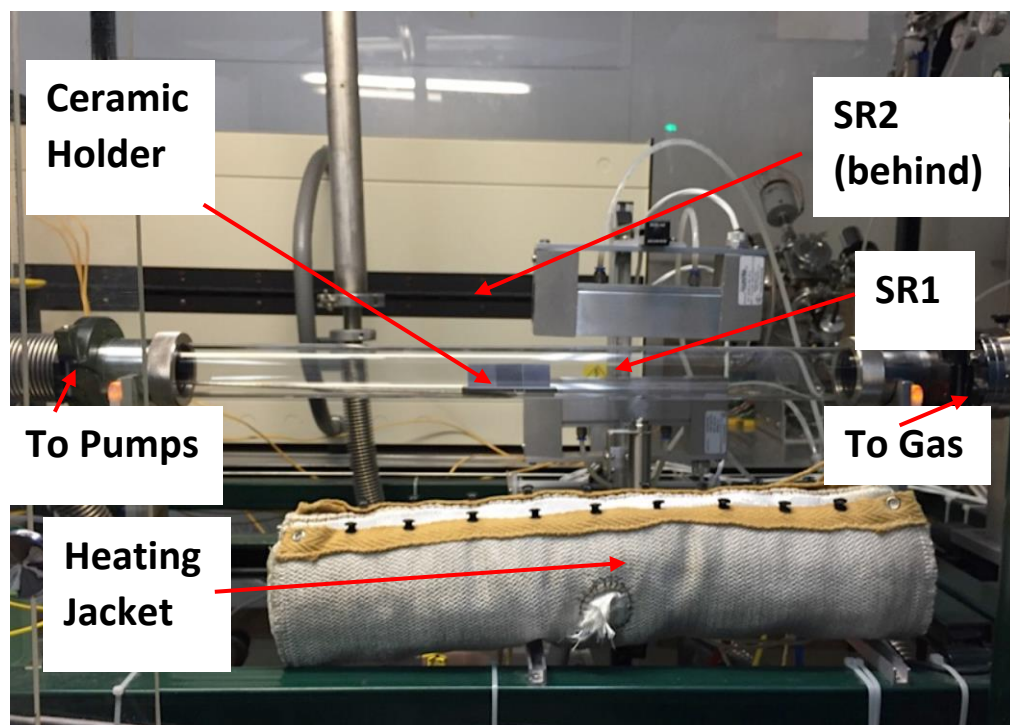


Figure 3.1: Picture of sulfurization/selenization system.

The reaction process for H_2S passivation begins by removing the SR1 tube and performing one last HF etch on the 1"x1" wafers to be reacted to remove any residual oxides. Then, the wafers are placed within a graphite holder that orients the samples vertically, as shown in Figure 3.1. Then, the tube is replaced, and pump down begins. SR1 pressure is brought to <15 mTorr via roughing pump, then brought below 10^{-6} Torr with a turbo pump. To begin the reaction itself, SR1 is filled with Ar to ~1 atmospheric pressure, then held at that pressure over a constant flow via the opening of a waste valve. Then, the reaction profile for the given experiment is executed, with additional process gas (H_2S , H_2Se or a mixture of H_2S and H_2Se) flow starting at 300°C as shown in Figure 3.2 and then heated to the target temperature at a rate of $\sim 15^\circ\text{C}/\text{min}$. The wafers are then

reacted for the target duration. Once the reaction is complete, the heating jacket is turned off, and allowed to cool naturally until 300°C, where the jacket is removed and the process gas flow is stopped. Once it is cooled down to $T \leq 35^\circ\text{C}$, three pump purges with Ar are performed to remove any hazardous gas still within the reaction chamber before it is brought back up to atmospheric pressure for sample removal and characterization.

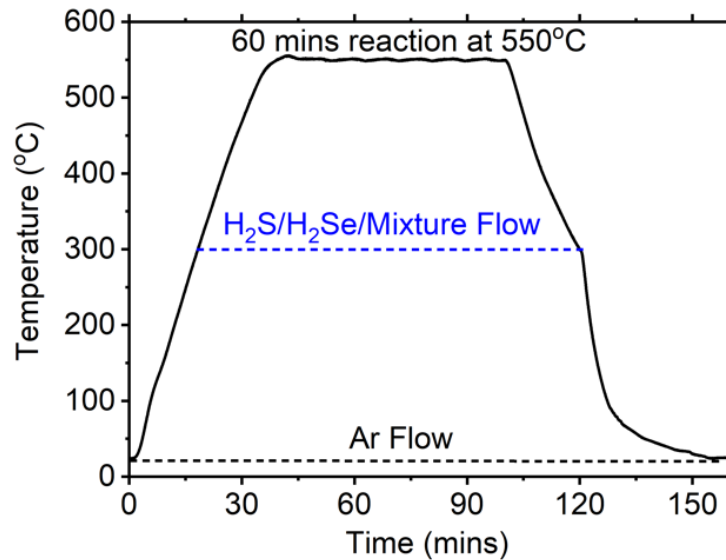


Figure 3.2: Typical time-temperature profile for 60 min reaction at 550°C.

3.4 Quasi-Steady State Lifetime Measurement

The first test for each reacted wafer sample is a quasi-steady state lifetime test, performed by a Sinton Lifetime Tester WCT-100. [37] The tester itself is a light source suspended above a platen with a sensor coil for measuring photoconductance, and a light sensor for measuring the intensity of the light. A typical quasi-steady state photoconductance (QSSPC) test is conducted as follows: the passivated sample is placed on top of the sensor coil and illuminated by a flash lamp, and the excess

photoconductance of the sample is measured. The light intensity is measured by a calibrated Si reference cell simultaneously. Under steady-state, the recombination and generation rates are equal, thus the recombination rate can be estimated (expressed as current density J_{ph}) as a function of the photoconductance (σ_L), then that and the dimensions of the wafer (thickness W) can be used to calculate the average minority carrier density (Δn_{av}) and the minority carrier lifetime (τ_{eff}) of the wafer according to: [37]

$$J_{ph} = \frac{\Delta n_{av} q W}{\tau_{eff}}; \sigma_L = q \Delta n_{av} (\mu_n + \mu_p) W; \tau_{eff} = \frac{\sigma_L}{J_{ph} (\mu_n + \mu_p)} \quad (3.1)$$

The quasi-steady state lifetime measurement (Figure 3.3) uses a long, slow light pulse that varies over time to collect lifetime data over a range of incident light current values. [38] The benefit of this method is that it allows measurement of very low lifetimes ($<10 \mu s$) when the minority carriers would normally be too spread out to get a consistent result. [37] This test has to be performed as fast as possible (ideally $< 1 \text{ min}$) after reaction, as the passivation layer oxidizes rapidly in open air (5 mins for half lifetime).

To explain Figure 3.3 in detail, the measurement of lifetime is split into two separate parts. First, the photoconductance of the wafer at each given time is compared against a standardized wafer used for calibration and is output as the red line (line A) in the top graph. For each of these time periods, the intensity of the light is also measured and plotted alongside the photoconductance response as the blue line (line B). These are the direct experimental results, which are then interpreted into the graph on the bottom. First, photoconductance is converted into minority carrier density using the σ_L equation above, holding μ_n and μ_p constant. Then, the average minority carrier density, the

thickness of the wafer, and the light intensity is used to calculate the photogeneration rate (J_{ph}), which is itself the recombination rate. From this, an effective lifetime can be calculated for each of the minority carrier densities and the bottom graph is created.

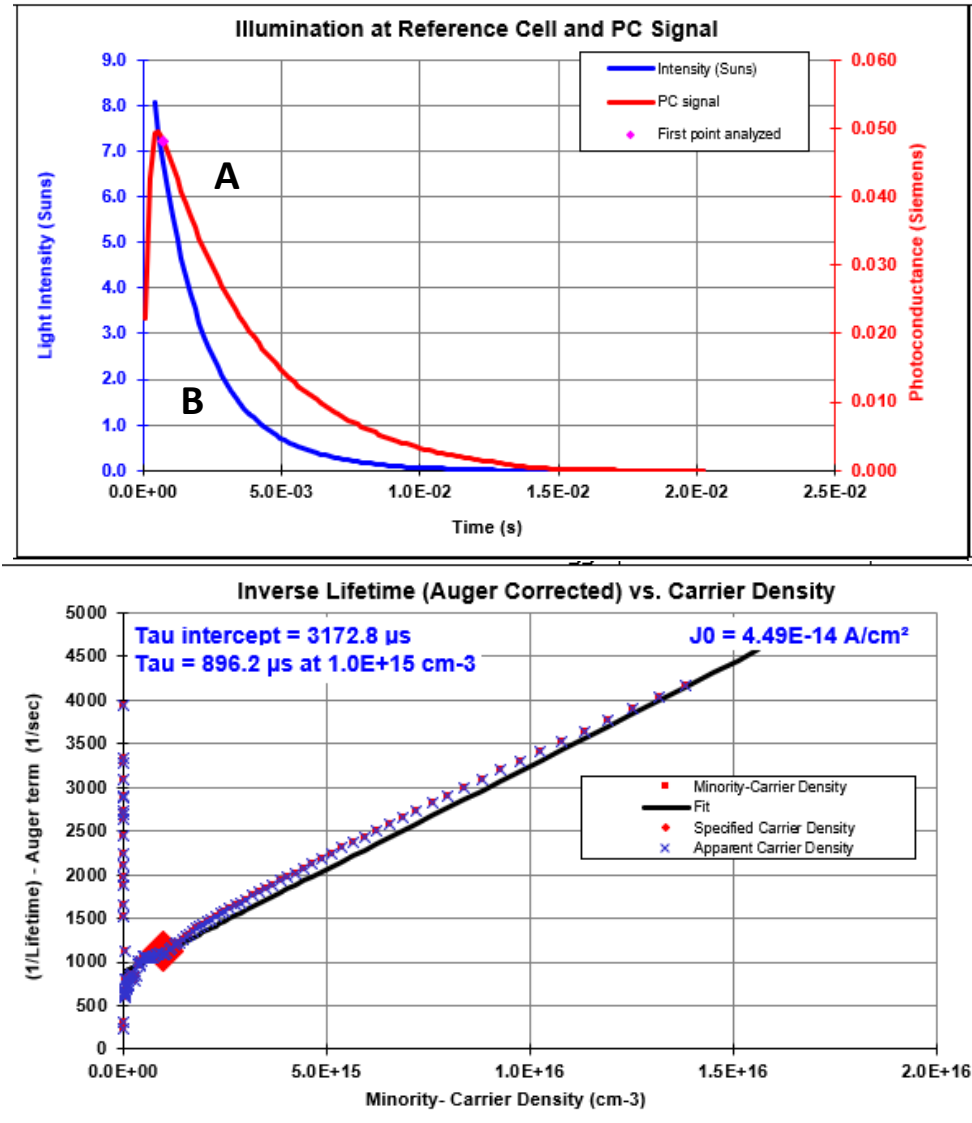


Figure 3.3: Suns-photoconductance curve (top) is interpreted into lifetime/carrier density curve (bottom).

There are two other important parameters used to characterize the reacted wafers: SRV will be the primary method of comparing undiffused wafers, as the wafer is assumed to be uniformly doped and normalized by wafer thickness. For this experiment, SRV is derived from lifetime, which is itself subject to adjustment. What the QSSPC measures is the effective lifetime (τ_{eff}), which combines the effects of both the surface layer and the bulk. In other words, to separate the lifetime within the surface, the bulk lifetime must be known. In order to estimate bulk lifetime, the y-axis intercept of the linear portion of the bottom graph (the straight black line) is used as the bulk lifetime (τ_{bulk}). Then, τ_s is obtained from equation 3.2 and SRV (S) is calculated with known wafer thickness (W). [11]

$$\frac{1}{\tau_{eff}} = \frac{1}{\tau_{bulk}} + \frac{1}{\tau_s} \rightarrow \frac{1}{\tau_s} = \frac{2S}{W} \quad (3.2)$$

J_0 (dark saturation current density or recombination current density) is another parameter that can be estimated from the quasi-steady state lifetime test and is very important when wafer surface is doped by additional doping than the bulk. This J_0 significantly affects solar cell V_{OC} . The higher this value is, the lower the resultant V_{OC} will be, so it is important to get J_0 as low as possible. This is not directly measured by any processes in this test, but it can be estimated from the slope of the minority carrier density curve in Figure 3.3.

$$J_0 = \frac{1}{2} q W n_i^2 \frac{d}{d\Delta n} \left(\frac{1}{\tau_{eff}} \right) \quad (3.3)$$

3.5 Sheet Resistance

Another parameter that will be used to categorize dopant-diffused wafers is the sheet resistance. The sheet resistance is necessary for designing the contacts in the final cell structure since minimizing resistance is important to minimizing power loss. The method that will be used in this project will be a simple 4-point probe method performed [39] on unpassivated Si n-n⁺ or n-p⁺ samples after they have been cleaned, but before they are processed for passivation. The sheet resistance is extracted from the voltage and current readings from the probe: $R_{sheet} \left(\frac{\Omega}{sq} \right) = \frac{\pi V}{\ln 2 I}$. As a result of the dopant layer (Figure 3.4), this reading includes interactions from multiple layers. Thus, the sheet resistance of the n⁺ layer can be extracted by knowing the sheet resistance of the base Si in addition to the measured value, which can be extracted by equation 3.4.

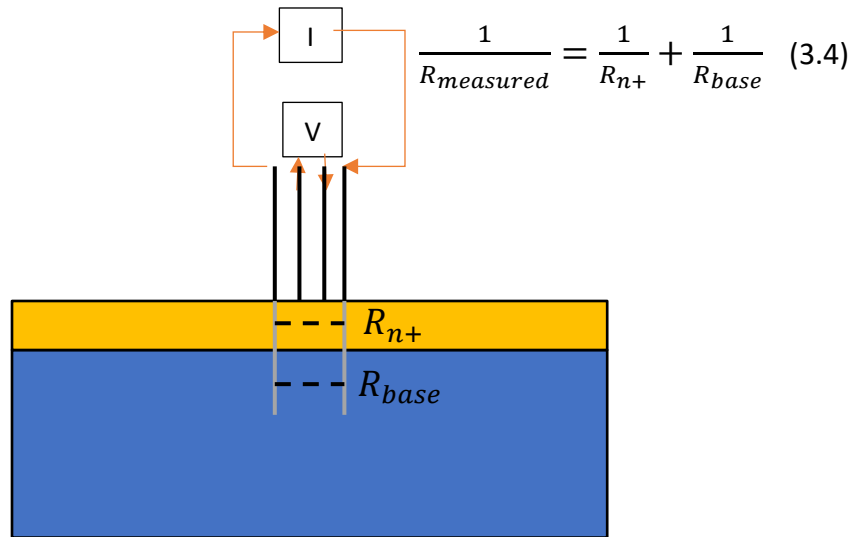


Figure 3.4: The structure of a dopant Si wafer as pertaining to a 4-point resistance measurement. The current travels in parallel in both regions.

3.6 SRH Formalism Modelling of D_{it} and Q_f

A modelling software developed by Shu was used to estimate D_{it} and Q_f of some of the S-passivated samples using lifetime curves generated by the QSSPC testing. [8] This program uses the lifetime vs. minority carrier density curves seen in Figure 3.3 and relates them to D_{it} and Q_f via an SRH formalism. The primary equation that it uses is as follows: [8]

$$SRV(\Delta n) = \frac{v_{th}(n_s p_s - n_i^2)}{\Delta n} \int_{E_v}^{E_c} \frac{D_{it}(E)}{\frac{n_s + n_1}{\sigma_p} + \frac{p_s + p_1}{\sigma_n}} dE \quad (3.5)$$

This equation varies D_{it} as a function of the energy state, and outputs an SRV or lifetime vs Δn curve that predicts how a wafer with given parameters would behave. [8] Though this paper applies the program to c-Si / a-Si:H interfaces, a similar theory was assumed for Si:SiS₂ interfaces. Under this SRH formalism, there are two separate areas where D_{it} is highest within the band gap: on the edges of the band gap where shallow states are assumed to be insignificant for recombination and the middle of the band gap where defect energy levels are the most effective recombination centers. [40] For the purposes of this thesis, the D_{it} and capture cross sections will be assumed constant across the entire band gap. This assumption is suitable for calculation of curves, because the states at the edges of the band gap do not contribute to SRH recombination significantly.

Chapter 4

RESULTS

4.1 Outline of Experiments

To begin, an effective wafer surface cleaning method was established based on minority carrier lifetime measurements with Si surfaces passivated by quinhydrone-methanol (QH) solution. Three different types of Cz Si wafers are investigated: semi polished n-type wafers already available at the IEC as a reference (SP-n) with high bulk quality n-type (same as in Liu's studies[2]), GT-n with lower bulk quality n-type than SP-n and GT-p p-type wafers. The wafer parameters and the results of surface cleaning studies are described in section 4.2.1.

Section 4.2.2 describes the comparison of SRV's of three types of wafers (SP-n, GT-n, and GT-p) with S-passivation achieved by reacting the wafers in 3.4% H₂S in Argon for 30 mins at different temperatures ranging from 400 - 650°C. The effective minority carrier lifetimes are measured within 2 minutes after the samples are removed from the reactor and SRV values are calculated assuming the bulk lifetime equal to the τ_{fit} from QSSPC measurements. τ_{bulk} was estimated from QSSPC measurements following the method reported in literature. As a first step, a linear fit of $1/\tau_{eff}$ vs excess carrier density (Δn) at high injection level is obtained and the slope is related to J_0 as shown by equation

4.1. Then τ_{bulk} is calculated from the slope and the dopant density of the wafers at low injection level using equation 4.2. This τ_{bulk} is referred to as “ τ_{fit} ”.

$$\left. \frac{1}{\tau_{\text{eff}}} \right|_{\text{high injection}} \approx \frac{2J_0}{qn_i^2 W} \Delta n \quad (4.1)$$

$$\left. \frac{1}{\tau_{\text{eff}}} \right|_{\text{low injection}} \approx \frac{1}{\tau_{\text{bulk}}} + \frac{2J_0}{qn_i^2 W} \frac{N_D}{A} \quad (4.2)$$

The specifics of these wafers are as follows (all 1”x1” Si wafers): SP-n n-type reference wafers (140 μm , 2 $\Omega\cdot\text{cm}$), GT-n n-type wafers provided by GIT (160 μm , 3 $\Omega\cdot\text{cm}$), and GT-p p-type wafers also provided by GIT (160 μm , 2 $\Omega\cdot\text{cm}$). The clean wafers were loaded into the quartz tube reactor and pumped to $< 10^{-6}$ Torr. The wafers were then reacted for 30 mins at temperatures ranging from 400°C to 650°C at atmospheric pressure with 3.5% H_2S in Ar ambient. The surface passivation quality was evaluated by minority carrier lifetime measurements by QSSPC on the wafers with S passivation right after the samples were removed from the reactor; this is reported as “initial lifetime”.

Section 4.2.3 is an investigation of the decay of S passivation on textured Si wafers by varying the reaction time, alongside separate experiments for stabilization with a-SiN_x. Samples at 550°C were reacted for 15, 30, 45, 60, 120, and 210 minutes. From these samples, QSSPC measurements are taken repeatedly over 40+ minutes after reaction while exposed to air, and a profile is made of how lifetime decays over time. The bulk lifetime is also recalculated, to see if the textured wafers are different in the bulk than the untextured wafers. After it was noted that the S passivation decays quickly, a-SiN_x was studied as a capping layer to stabilize the passivation. This process was studied by depositing 70 nm of a-SiN_x at 350°C in a PECVD process immediately after

passivation. These samples are then measured for lifetime, then placed in a desiccator and remeasured regularly to determine decay over more than two months.

Section 4.2.4 is an exploration of the effects of flow rate and H₂S concentration on lifetimes. This series of tests varied both total gas flow and H₂S concentration in Ar, while keeping temperature and reaction time constant at 550°C and 60 min, respectively. The combinations tested are listed in Table 4.1 below. S1458 is the normal baseline determined previously with Ar flow rate = 1290 sccm, while the rest are in relation to this reference. Due to limitations in the maximum flow rate of a given gas imposed by the MFC controllers, some combinations could not be tested.

Table 4.1: Experimental design for concentration and gas flow.

Batch Name	H ₂ S Concentration (%)	Ar Flow Rate (Relative to S1458)
S1458	3.4	Normal
S1459	1.7	Normal
S1460	6.5	Half
S1465	3.4	Half
S1466	1.7	Double
S1467	0.9	Double
S1468	0.5	Double

Section 4.2.5 will explore the passivation of Si with selenium. Se passivation tests were carried out in a very similar manner to the previous sulfur passivation tests, varying reaction temperature and keeping reaction time constant at 60 min. Due to poor Se

passivation performance by itself, mixtures of S and Se were explored (keeping total flow rate constant).

Section 4.2.6 will proceed with the passivation of dopant diffused n-n⁺ and n-p⁺ wafers and determine if any changes needed to be made to the passivation process. To determine the ideal cleaning procedure for dopant diffused n-n⁺ and n-p⁺ wafers to achieve complete removal of surface oxide and hydrophobic surface prior to sulfur passivation, three types cleaning processes were investigated: (a) a 2 – 4 s etch clean in 100:1 HNO₃:HF solution (HNA) followed by piranha oxidation and final oxide etch in HF; (b) piranha oxidation followed by oxide etch in HF; and (c) only HF dip without any chemical oxidation step. It is noted that the HNA etch clean process used here leaves behind a surface oxide layer due to excess HNO₃ in the solution.

Table 4.2 lists the different surface cleaning methods and passivation processes used for both p⁺ and n⁺ diffused n-type wafers. For surface passivation by sulfur, the wafers are loaded into the H₂S reactor immediately after the cleaning steps, pumped down to < 1x10⁻⁶ Torr, and performed passivation reaction at 550°C for different duration and H₂S concentration in Ar. In case of the surface passivation by the quinhydrone – methanol (QH-ME) solution, the cleaned wafers are immersed in the QH-ME solution for ~ 15 mins before the QSSPC measurements for J₀.

Table 4.2: Surface cleaning and passivation steps studied for n⁺ and p⁺ diffused n-type Cz Si wafers.

Cleaning Steps	Passivation process	Process name
HNA etch (2 – 4 s) + Piranha oxidation + HF etch	H ₂ S reaction, 60 mins	HNA-P-HF
Piranha oxidation + HF etch	H ₂ S reaction, 60 mins	P-HF
HF etch	H ₂ S reaction, 60 mins	HF-60
HF etch	H ₂ S reaction, 30 mins	HF-30
HF etch	H ₂ S reaction, 15 mins	HF-15
HF etch	2 x H ₂ S flow, 60 mins	HF-2S
HF etch	QH-ME solution	HF-QH

Section 4.2.7 will connect the experimental results with the fixed charge density and surface state density, with modelling of previous samples done with a program built by Brent Shu. [8] This program uses the lifetime vs. minority carrier density curves seen in Figure 3.3 and relates them to D_{it} and Q_f via an SRH formalism. [8] Though this paper applies the program to c-Si / a-Si:H interfaces, a similar theory is applied to Si:SiS₂ interfaces. An example fitting is shown in figure 4.1. Three series will be analyzed: a reaction temperature, a passivation decay in air, and a concentration series, as listed in table 4.3. The capture cross section ratio (σ_p/σ_n) is held constant at ~12.

Table 4.3: Analyzed samples for modelling of D_{it} and Q_f .

Series	Samples
Temperature	S1356 (475°C), S1346 (500°C), S1345 (550°C), S1340 (600°C), S1347 (650°C)
Decay	S1383 (through 12 min)
Concentration	S1458 (3.4 % H ₂ S), S1460 (6.8% H ₂ S), S1466 (1.7% H ₂ S), S1467 (0.8% H ₂ S)

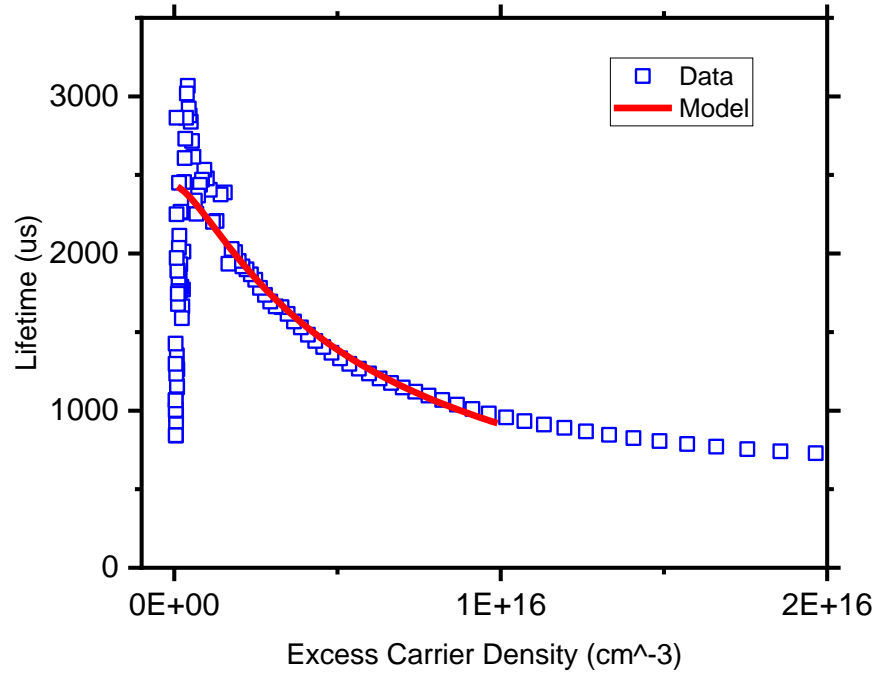


Figure 4.1 Example fitting using a program made by Brent Shu. [8]

4.2 Final Results

4.2.1 QH Confirmation of Wafer Cleaning

To establish an effective cleaning procedure for the undiffused c-Si wafers, a series of wafers underwent two versions of the cleaning procedure, then investigated for surface passivation quality in QH-ME solution. Table 4.4 compares the effective lifetime obtained from QSSPC measurements of 3 types of wafers in QH-ME solution using the two different cleaning processes.

Table 4.4: Effective minority carrier lifetime (τ_{eff}) at excess carrier density of $1 \times 10^{15} \text{ cm}^{-3}$ for SP-n, GT-n and GT-p wafers with and without the HNA steps. The values are averaged over 3 wafers for each type.

Wafer	$\tau_{eff} (\mu\text{s}) @ 10^{15} \text{ cm}^{-3}$	
	No HNA etch	60 s HNA etch
SP-n	1500 ± 200	2200 ± 300
GT-n	460 ± 100	970 ± 200
GT-p	170 ± 50	180 ± 50

The data shows improved lifetime for the wafers that were cleaned with HNA etch, indicating better surface cleanliness and passivation quality as compared to the wafers without the HNA etch.

4.2.2 Surface passivation by H₂S Reaction at Different Temperatures

To confirm results from Liu et al. [2] that S could passivate silicon, the passivation of planar and textured surfaces on n and p-type Cz Si wafers by H₂S reaction was carried out. There are multiple variables that can influence the final performance of the wafer, including the reaction time, the temperature at which the process is performed (including rate of heating and cooling), and the type and amount of process gas used to passivate the sample. The purpose of this series of tests is to optimize the reaction temperature and re-establish Liu's surface passivation results on high bulk quality n-type wafers (SP-n).

In terms of optimizing the time-temperature profile of the passivation procedure, there was little change from Liu et al. [10] Performing the process at 550°C was found to

be the optimal in terms of lifetime and SRV for S passivation [Figure 4.2] and similar to the results reported by Liu et al. [34] At the ideal temperature, S passivation can reduce SRV to less than 2 cm/s. In terms of stability, the SRV of a given sample rapidly increases when exposed to air. [Figure 4.3] In addition, the bulk lifetimes of each wafer are established via the process established in section 3.3 [Figure 4.4] with τ_{fit} of 10000, 4000, and 400 μ s for SP-n, GT-n, and GT-p, respectively.

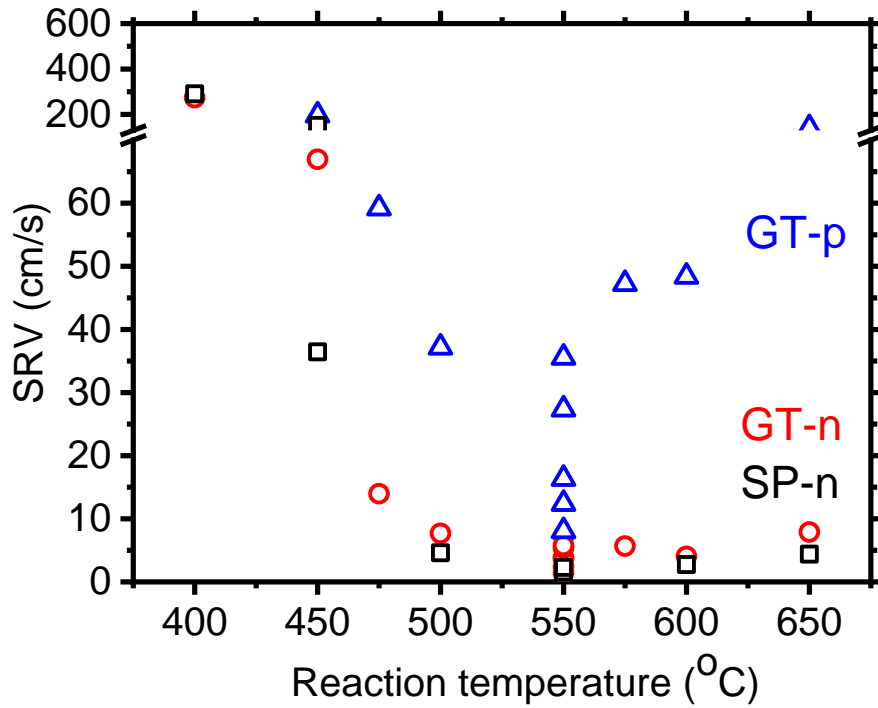


Figure 4.2: Temperature optimization for H₂S passivation at 3.4% in Ar concentration.

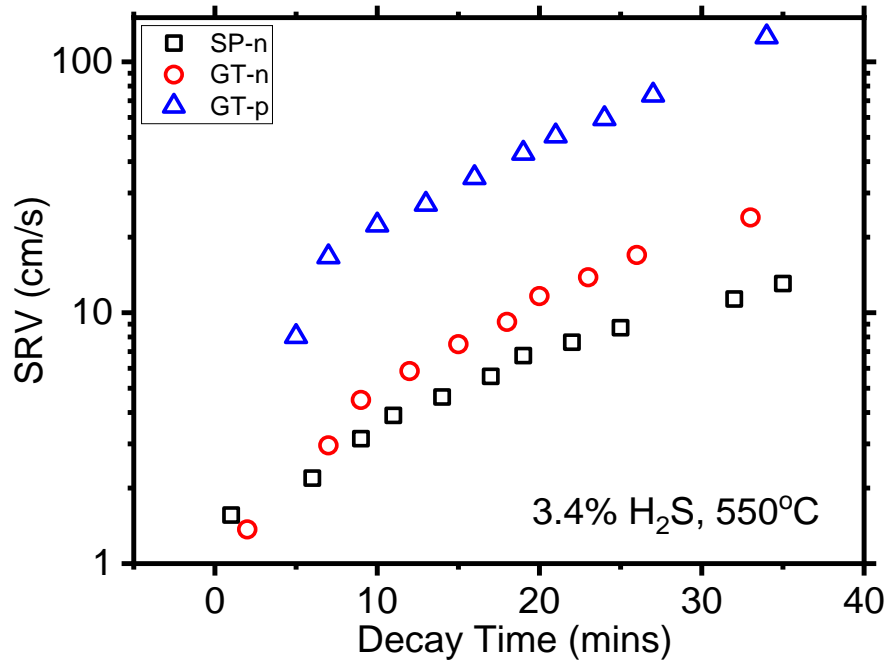


Figure 4.3: Initial degradation study of GT-n, GT-p, and SP-n wafers.

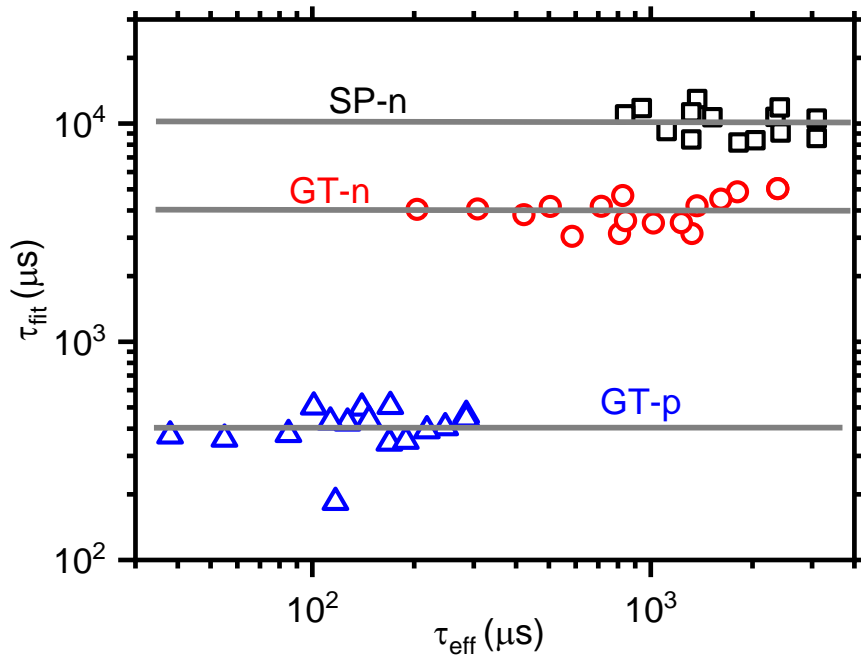
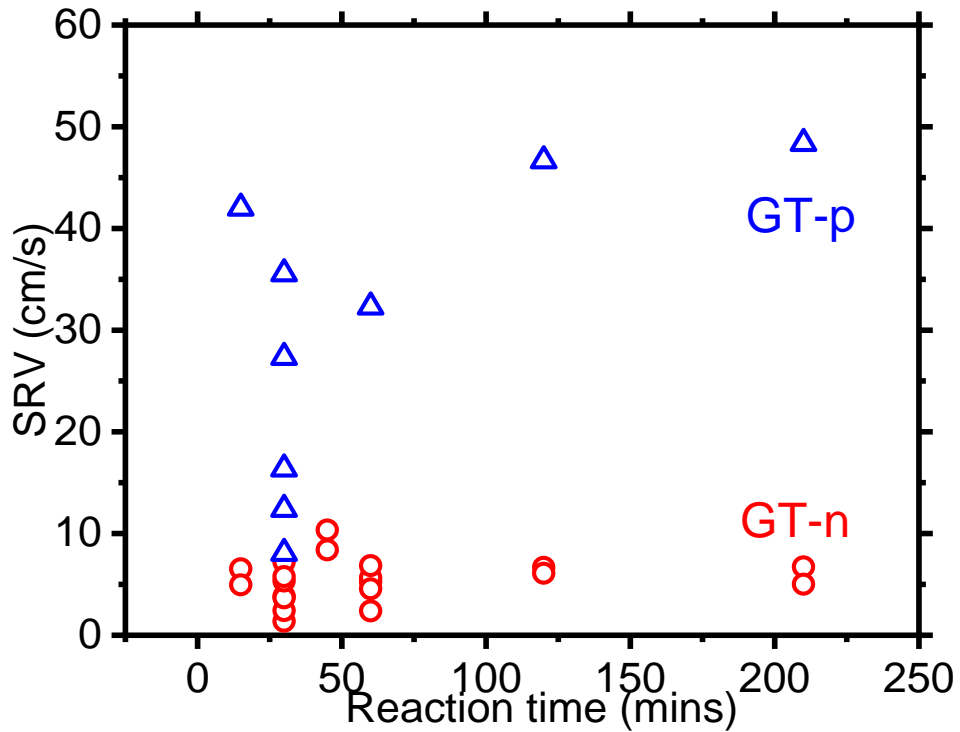


Figure 4.4: Relationship between τ_{fit} and τ_{eff} . Averages for τ_{fit} are shown for each type of wafer, and estimates of τ_{bulk} .

4.2.3 Reaction Time and SRV Stability

As an extension of the previous experiments, these experiments were repeated on textured n and p-type Si wafers. By varying the length of the reaction at the ideal temperature, it was found that longer reaction times can increase the stability of the passivation. [Fig. 4.5a] 60 minutes at 550°C was found to be the time and temperature profile with the best combination of performance and stability, with higher times increasing the stability of the S passivation, and lower times reducing it. [Fig 4.5b]



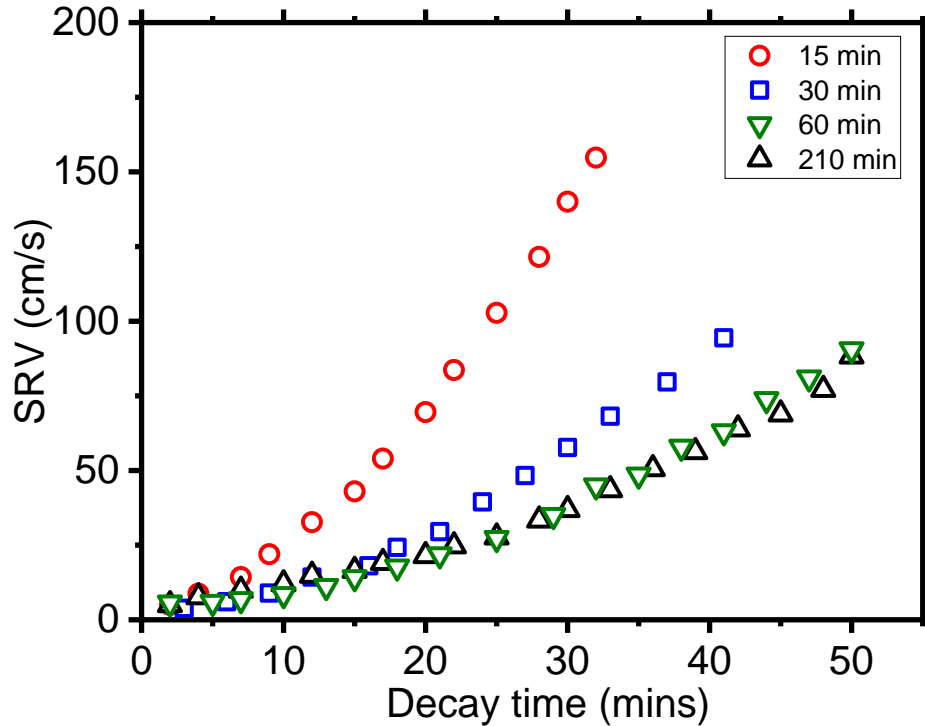


Figure 4.5 (Top, a) Lifetime as a function of reaction time for n-type and p-type textured Cz Si wafers. (Bottom, b) Degradation of lifetime of S passivated GT-n and GT-p wafers show slower degradation rate for longer reaction time irrespective of wafer types and surfaces.

To further stabilize this structure, a capping layer of a-SiN_x has been found to improve the stability of a S passivation layer [Figure 4.6]. This is a ~100 nm thick SiN_x layer deposited at 350°C after minimum air exposure (~ 2 mins). While normally the S passivation decays in minutes, the a-SiN_x layer helps keep it stable over a period of months. This stability persists after firing, though with degraded performance. The firing process was a 740-770°C annealing for ~30s in an industrial belt furnace on day 90. [Figure 4.7] This subject would be expanded upon with dopant diffused wafers.

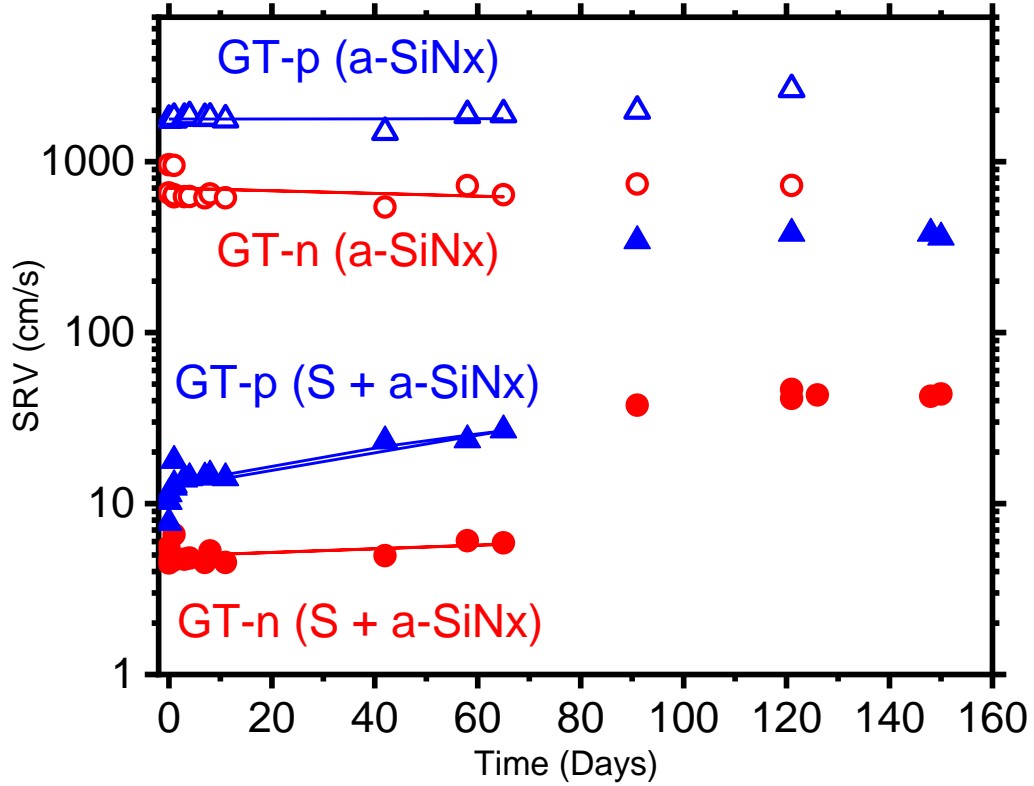


Figure 4.6: Long-term stability of a-SiN_x capping layer with/without H₂S passivation. Linear regressions pre-firing model degradation. Linear Periods after day 90 are post-firing, according to Figure 4.7.

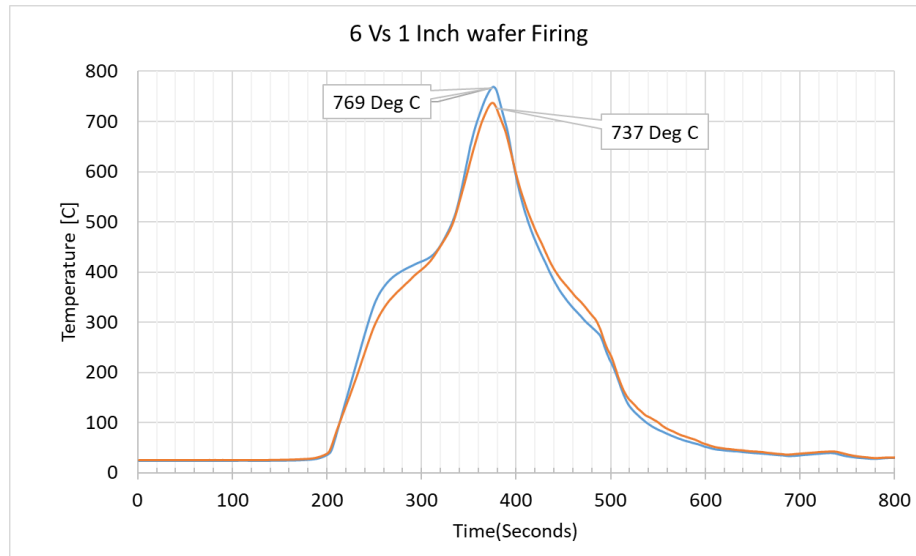


Figure 4.7: Sample temperature curve for GIT firing process (from GIT).

4.2.4 S Concentration, Flow Rate

In this experiment set, H₂S concentration in Ar is varied from 0% to 6.5% on n-type and p-type Si. [Fig 4.8] The concentration range is, however, limited by the H₂S MFC flow (limited to 45 sccm) and the total flow rate required for the atmospheric pressure process. To elaborate, the base Ar flow is 1290 sccm, with a maximum of 3000 sccm. A total of seven experiments were performed, shown in Table 4.3. For these experiments, the concentration of Ar is much higher than that of H₂S so the total flow rate is largely controlled by that of the Ar, while the H₂S flow rate could be changed without significantly impacting the overall flow rate.

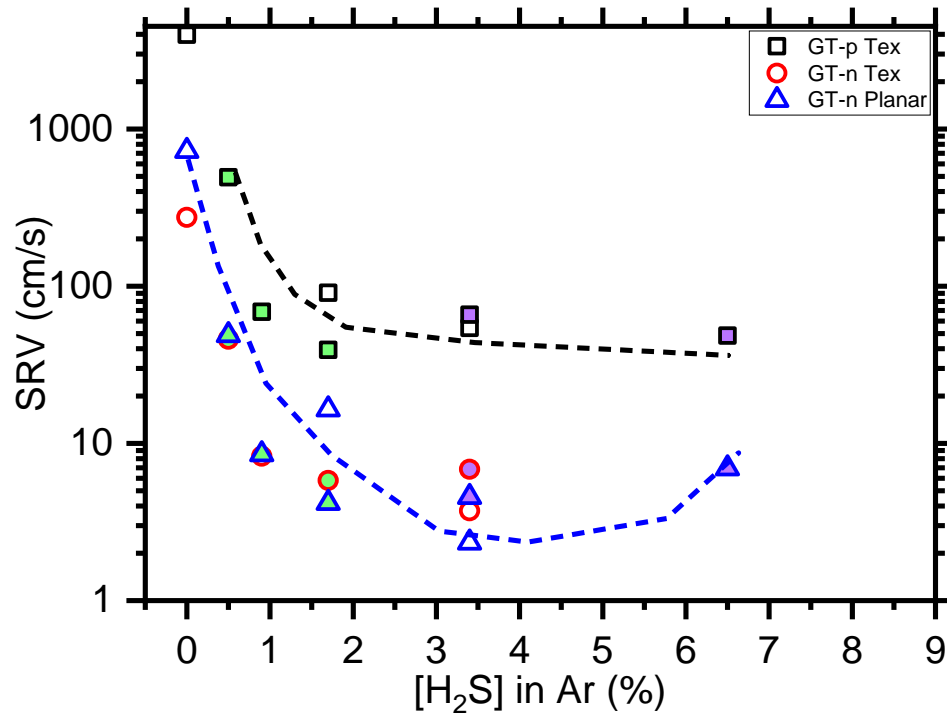


Figure 4.8: Gas flow and concentration in H₂S passivation. A green filled data point is at double flow rate, and a purple filled data point is at half flow rate.

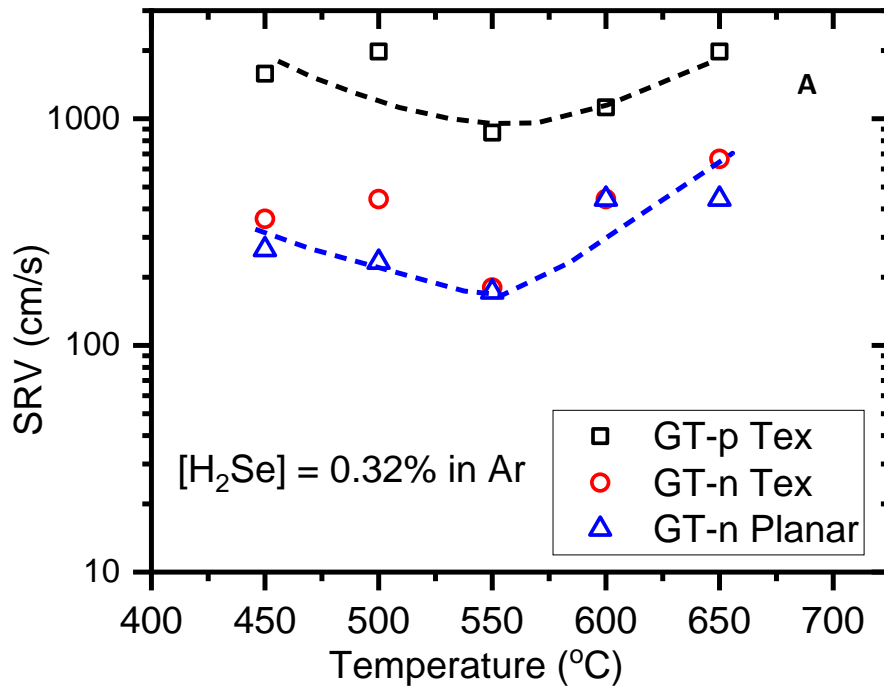
A reaction in 3.4% H₂S exhibits the best passivation quality, with a notable SRV of 2.3 cm/s and 3.7 cm/s on GT-n-type planar and textured wafers respectively. This passivation quality by S is similar or better than the standard thermal oxide/SiN and ALD Al₂O₃/SiN passivation quality, SRV's of which are shown in Table 4.5. Another observation is that increasing the Ar flow rate (comparing S1459 and S1466) can provide a significant boost to passivation quality, with SRV dropping from ~20 cm/s to < 6 cm/s at a H₂S concentration of 1.7%. An SRV < 10 cm/s is achieved even at the H₂S concentration of 0.9% (S1467) by doubling the Ar flow rate.

Table 4.5: Surface Passivation quality of sulfur passivation results as compared to Al₂O₃ (ALD) and thermal oxide passivation.

Type	Surface	Passivation	Post Passivation/pre Firing		Post Firing	
			SRV (cm/s)	t _{eff} (ms)	SRV (cm/s)	t _{eff} (ms)
N-Cz (1-10 ohm)	Textured	ThermalOx/SiN	3.0	1690	6.8	612
		ALD/SiN	2.1	387	3.8	456
		Sulfur	3.7	1398	--	--
	Planar	ThermalOx/SiN	4.6	412	4.1	800
		ALD/SiN	7.8	181	3.9	630
		Sulfur	1.9	1843	14.2	202
P-Cz (1-3 ohm)	Textured	ThermalOx/SiN	2.3	307	4.0	306
		ALD/SiN	5.6	224	5.7	86
		Sulfur	33.1	135	--	--
	Planar	ThermalOx/SiN	6.4	386	1.0	587
		ALD/SiN	11.2	242	2.3	534
		Sulfur	11.7	247	307.5	22

4.2.5: Se Passivation and S/Se Mixtures

In terms of selection of passivation material, S-passivation has produced SRV values under 3 cm/s, while Se has shown some passivation but remains much inferior than S passivation with SRV values above 100 cm/s. It is to be noted that the Se-passivation is performed at a very low H_2Se concentration of 0.32% in Ar. Attempting to increase the H_2Se concentration in otherwise the same process conditions leads to a thick metallic Se deposit in the cooler regions of the reactor. Therefore, we have performed experiments with a mixture gas of H_2S and H_2Se . Any amount of Se, even in a mixed gas reaction, [Fig. 4.9a and b] increases SRV and thus reduces the performance of the passivated wafer. This indicates that the Se is less effective for Si surface passivation in our current atmospheric pressure reactor design.



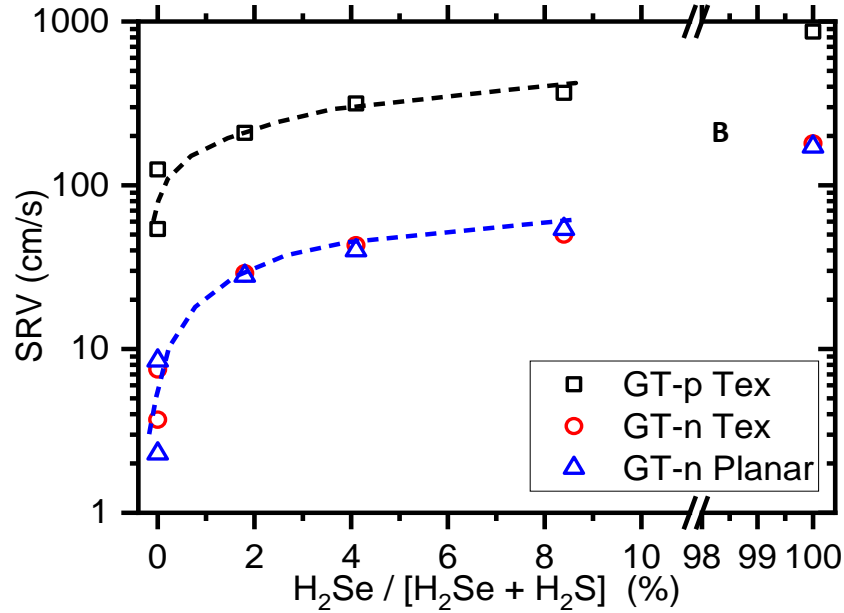


Figure 4.9: (Top,a) SRV as a function of reaction temperature at 0.32% in Ar (Bottom,b) SRV as a function of H₂Se concentration in an H₂Se/H₂S gas mixture.

4.2.6 Diffused Wafer Passivation

Figure 4.10 shows the variation of J_0 values with different surface cleaning and passivation processes listed in Table 4.6 for (top) boron diffused n-type (n-p⁺) wafers and (bottom) phosphorus diffused n-type (n-n⁺) wafers, respectively. The state-of-the-art J_0 values measured by GIT after the simulation firing for n-p⁺ is < 30 fA/cm² and for n-n⁺ is 35 fA/cm², and are represented by “star” symbol in the figures. It is to be noted that the state-of-the-art passivation stack for n-p⁺ wafers are ALD Al₂O₃ / SiN_x and for n-n⁺ wafers are thermal SiO₂ / SiN_x, as described in Table 4.2. Any oxidation step via HNA and/or piranha cleaning prior to S-passivation is found to be detrimental for n-p⁺ wafer surface passivation with high J_0 . A simple HF clean prior to S-passivation leads to $J_0 > 1000$ fA/cm², which remains unchanged even for longer H₂S reaction time and higher

concentration. However, n-p+ wafers surface cleaned by HF and passivated by QH-ME solution exhibit excellent passivation quality with $J_0 < 20 \text{ fA/cm}^2$, similar to the state-of-the-art passivation provided by ALD $\text{Al}_2\text{O}_3/\text{SiN}_x$ stack with simulation firing. This suggests that the current H_2S reaction process is unable to provide much passivation of n-p+ surface and suggests further surface characterization of Q_f , D_{it} and surface bonding are needed to characterize the mechanism.

Table 4.6: Dopant-diffused wafers used for sulfur passivation. J_0 and implied V_{oc} were estimated from QSSPC before S/Se process.

Type	R_{sheet} (Ω/sq)	Passivation	Purpose	J_0 (fA/cm^2)	Implied V_{oc} (mV)	Measured at
n+ (POCl_3)	70→ 106	8nm SiO_2/SiN	Verification for J_0 estimation	35	686	GIT
				33	678	IEC
	72	None	For S/Se process	840	613	IEC
	72→106	8nm SiO_2	For SiO_2 removal and S/Se process	70	669	IEC
	72→ 108	16nm SiO_2		85	665	IEC
p+ (APCVD B)	199	None	For S/Se process	1605	591	IEC

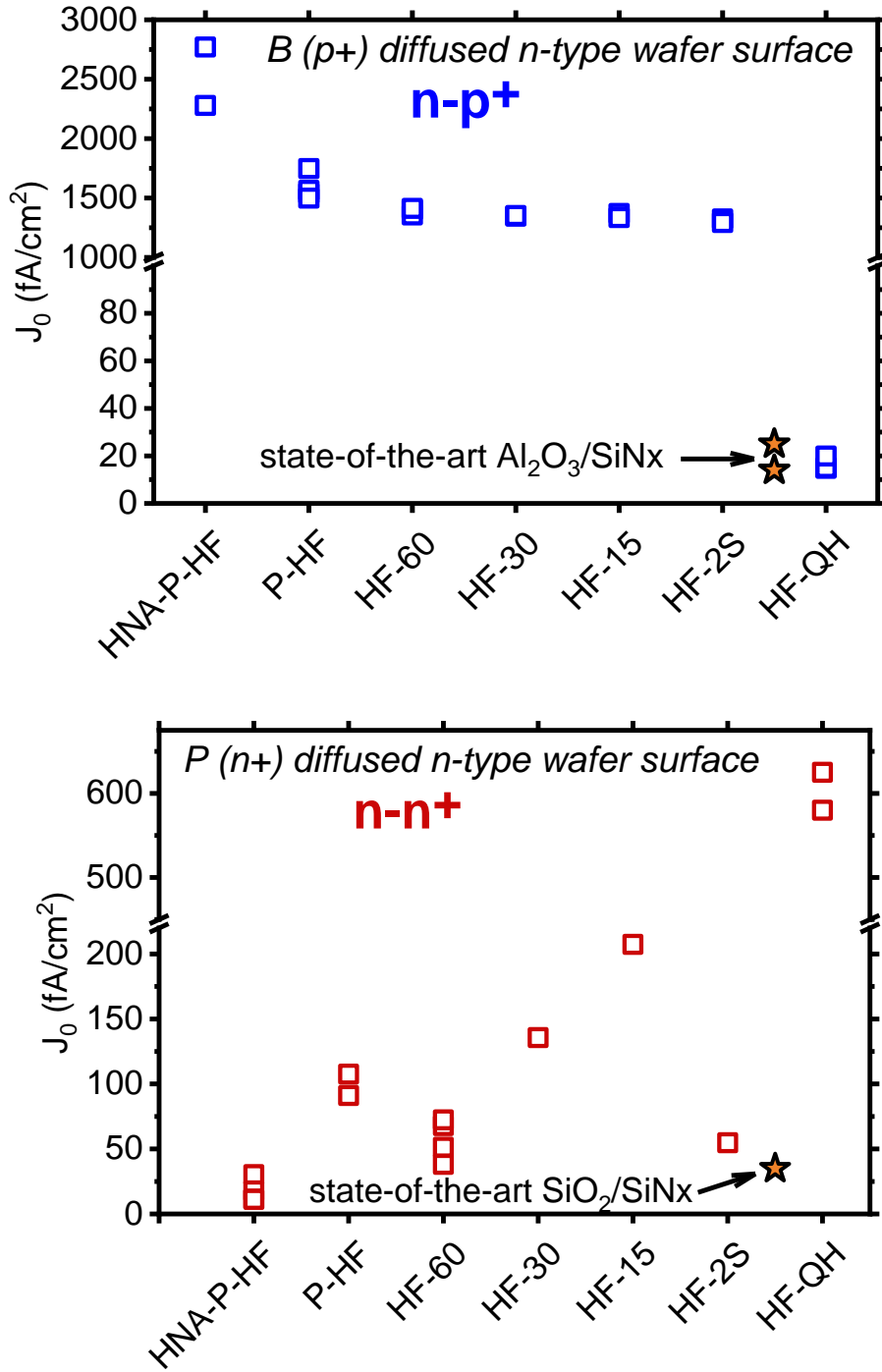


Figure 4.10: $n-p^+$ (Top) and $n-n^+$ (Bottom) S surface passivation with different cleaning and passivation processes.

On the contrary, the same cleaning and passivation processes using H₂S reaction on n-n⁺ wafer surface results in excellent passivation with J₀ as low as 38 fA/cm² that is comparable to the state-of-the-art passivation (J₀ = 35 fA/cm²) provided by a thermal SiO₂/SiN_x stack after a firing step. It is also observed that the QH-ME solution does not passivate n-n⁺ wafers surface as well as it passivates n-p⁺ surface. The opposing passivation properties of H₂S reaction and QH-ME solution on n-p⁺ and n-n⁺ wafers are interesting but require detailed investigation and characterizations to unravel the underlying passivation mechanism.

A stability study was performed on these wafers using a similar a-SiN_x capping layer concept. [Fig 4.11] Again, this is by depositing a ~100 nm thick SiN_x capping layer at 300 - 350°C with ~ 2 min air exposure between the S-passivation and capping layer process. The changes in J₀ values with time in air are plotted in Fig.4.9 for three n-n⁺ wafers passivated by three different layers. The wafer passivated by just S shows an initial value of J₀ = 30 fA/cm² that rapidly degrades in air with J₀ increases by almost an order of magnitude in 20 mins. The application of a SiN_x capping layer on the S-passivated sample stabilizes the J₀ = 50 fA/cm² with no detectable degradation over two and half weeks. The sample with just the SiN_x passivation (without the S-layer) also exhibits a stable J₀ but with much higher value of ~ 180 fA/cm².

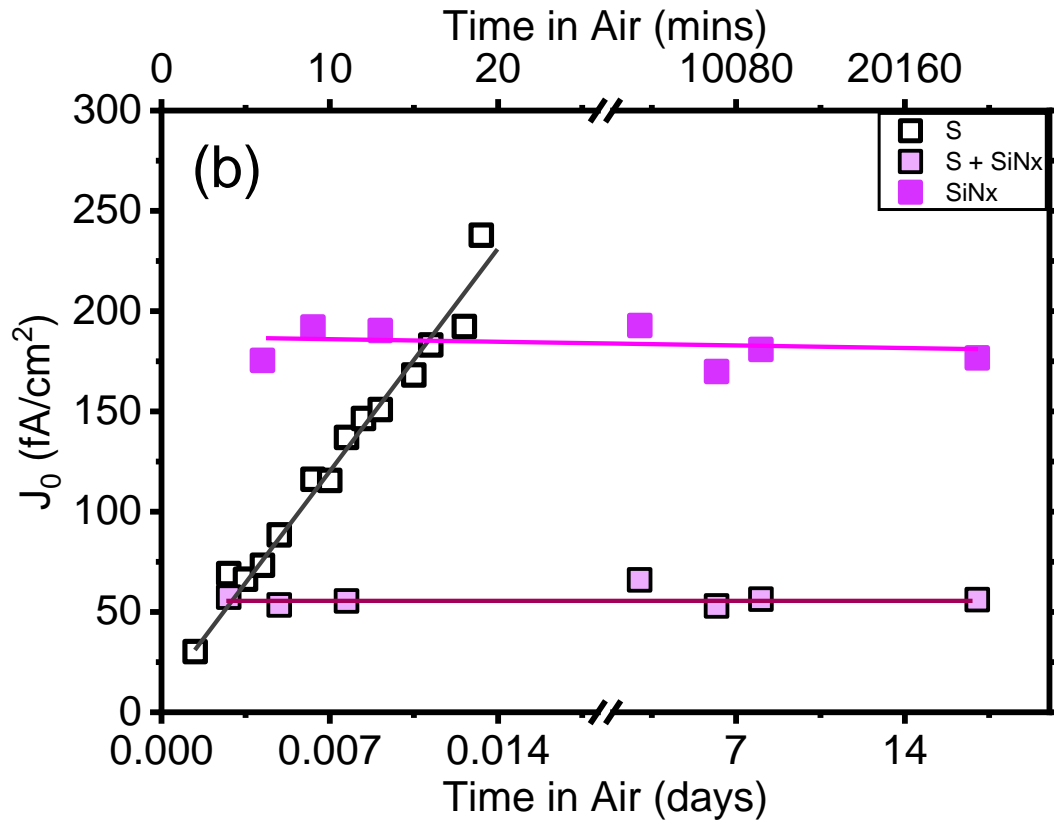


Figure 4.11: Stability of S passivation with/without a-SiN_x capping layer on dopant-diffused Si wafers. The HF-60 cleaning/reaction process used.

To continue the thermal stability study started with the undiffused Si wafers, a series of dopant diffused Si wafers were created and stabilized with a-SiN_x, varying the deposition conditions of the nitride layer as in Table 4.7. The PECVD SiN_x layers are deposited at two different temperatures (350 and 300°C) with two thicknesses (98 nm and 30 nm). The thinner SiN_x layer are further thickened to ~ 100 nm by GIT using their established PECVD process before subjection to the simulation firing step. This is so that experimental processes for a-SiN_x deposition can be compared. The results of these firing steps are recorded in Table 4.7. Performance after firing degrades significantly when only

using a-SiN_x from IEC, with low temperature deposition offering poorer relative performance before and after firing. The samples that have been combined with a-SiN_x deposited at GIT have a very different result, with J₀ improving significantly. Figure 4.12 compares the initial J₀ values recorded in Table 4.6 after passivation to R_{sheet} values of the base wafer. In comparison to the state-of-the-art thermal oxide passivation, most S + a-SiN_x wafers have a higher J₀ and a lower sheet resistance. However, there are some S passivation samples that are comparable to state-of-the-art thermal SiO₂ passivation before firing, and samples supplemented with GIT PECVD a-SiN_x have the closer values after firing.

Table 4.7: J_0 values of Si dopant-diffused n-n⁺ wafers passivated at 550 C by 3.5% H₂S.

Cleaning process	S-passivation ID	SiN _x deposition ID	SiN _x deposition temperature (°C)	SiN _x thickness (nm)	J_0 (fA/cm ²)	J_0 (fA/cm ²) after firing
P-HF	S1518-01	MC1732-01	350	98	103	371
HNA-P-HF	S1518-02	MC1732-02			56	760
P-HF	S1518-03	MC1732-03			123	680
P-HF	No Sulfur	MC1732-04			177	428
HF-60	S1524-01	MC1733-01	300	98	88	339
P-HF	S1524-02	MC1733-02			71	403
P-HF	S1524-03	MC1733-03			42	623
P-HF	No Sulfur	MC1733-04			475	851
P-HF	S1525-01	MC1734-01	300	30 nm IEC SiN _x + 70nm GIT SiN _x	86	67
P-HF	S1525-02	MC1734-02			50	64
P-HF	S1525-03	MC1734-03			47	49
P-HF	No Sulfur	MC1734-04			393	48
P-HF	S1526-01	MC1735-01	350	30 nm IEC SiN _x + 70nm GIT SiN _x	79	93
P-HF	S1526-02	MC1735-02			50	106
P-HF	S1526-03	MC1735-03			47	90
P-HF	No Sulfur	MC1735-04			293	52

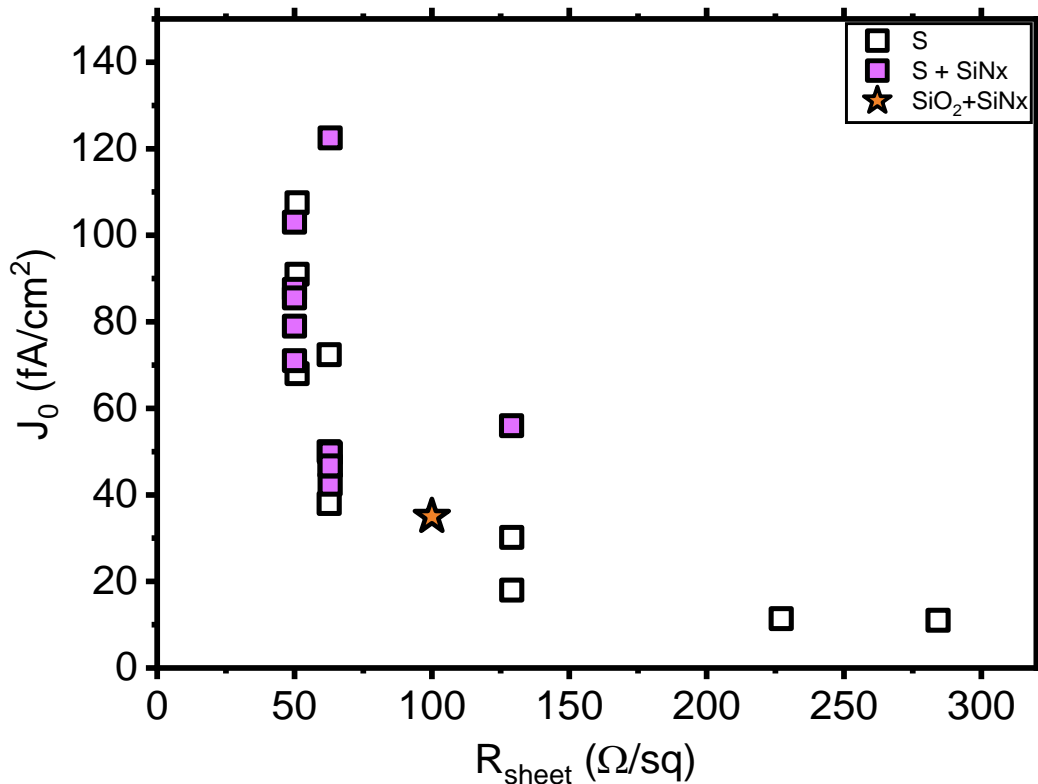


Figure 4.12: Relationship between J_0 and r_{sheet} on n-n $^+$ Si wafers.

4.2.7 Lifetime Modelling for D_{it} and Q_f

For this project, the capture cross section ratio is held constant, while D_{it} and Q_f are the main fitting variables. The ratio between hole and electron cross sections is very important, as the rate of recombination is highest when $\sigma_p p_s = \sigma_n n_n$. [8] When σ_p is not comparable to σ_n , this changes where the recombination happens and what mechanism. The maker of the software being used for this modification had experimentally measured D_{it} and Q_f , and used the program to fit σ_p and σ_n for a-Si/c-Si heterojunction (HJ) passivation. The direct measurement of many of the values mentioned previously come

from variations of CV testing, [41] with the cross-sections being the most difficult to measure. However, the creation of a reliable MOSFET structure using S passivation to perform the C-V and variant testing could take more time than is available. Thus, pre-existing values for HJ passivation are used as educated guesses for the capture cross-sections. Values from literature for Si have σ_p at least an order of magnitude higher than σ_n . The precise values are listed below in table 4.8, with a $\sigma_p/\sigma_n \approx 12$.

The D_{it} and Q_f values obtained from this model are listed in table 4.8. In the temperature and decay series, it is clear that D_{it} and Q_f both increase as the lifetime of the wafer decreases. In context, this means that the 550°C sample in the temperature series has the lowest D_{it} and Q_f , [Fig. 4.13 top] while in the decay series D_{it} and Q_f increase with time [Fig 4.13 bottom]. The very best sample has $D_{it} = 3.8 \times 10^{10} \text{ cm}^{-2} \text{ eV}^{-1}$ and $Q_f = 2.5 \times 10^{11}$. The worst result comes from heavy decay, with D_{it} and Q_f values far above reasonable estimates (1.5×10^{12} and 1×10^{12} , respectively).

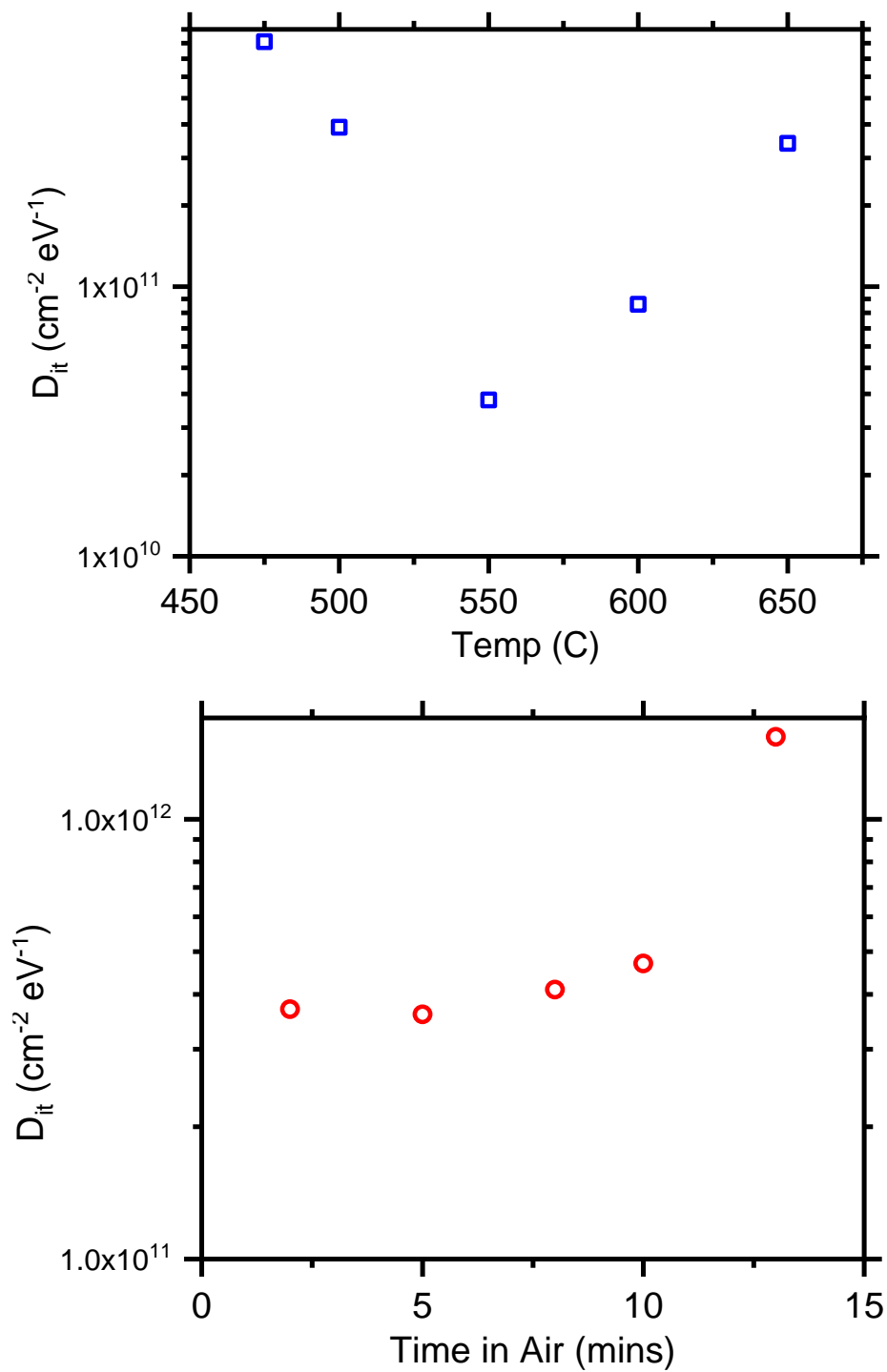


Figure 4.13 Estimated D_{it} values as a function of reaction temperature (top) and decay time (bottom).

Table 4.8: Extracted D^{it} and Q_f from lifetime modelling.

Sample	Type	Series			D_{it} (cm ⁻² eV ⁻¹)	Q_f (cm ²)	Life- time (μ s)	σ_p (cm ⁻²)	σ_n (cm ⁻²)
Reaction temperature series									
			Temp (C)						
S1345	n-pol	Temp	550		3.8×10^{10}	1.5×10^{11}	2375	4×10^{-18}	5×10^{-17}
S1346	n-pol	Temp	500		3.9×10^{11}	3.8×10^{11}	827	5×10^{-18}	6×10^{-17}
S1356	n-pol	Temp	475		8.1×10^{11}	6.0×10^{11}	501	6×10^{-18}	7×10^{-17}
S1340	n-pol	Temp	600		8.6×10^{10}	1.8×10^{11}	1325	6×10^{-18}	7×10^{-17}
S1347	n-pol	Temp	650		3.4×10^{11}	3.5×10^{11}	809	6×10^{-18}	7×10^{-17}
Lifetime decay series									
			Reading #	Decay (min)					
S1383	n-tex	Decay	0	2	3.7×10^{11}	3.8×10^{11}	989	5×10^{-18}	6×10^{-17}
	n-tex	Decay	1	5	3.6×10^{11}	3.7×10^{11}	813	5×10^{-18}	6×10^{-17}
	n-tex	Decay	2	8	4.1×10^{11}	4.0×10^{11}	799	5×10^{-18}	6×10^{-17}
	n-tex	Decay	3	10	4.7×10^{11}	4.2×10^{11}	770	5×10^{-18}	6×10^{-17}
	n-tex	Decay	4	13	1.5×10^{12}	1.0×10^{12}	645	5×10^{-18}	6×10^{-17}
H ₂ S concentration series									
			Flow	H ₂ S %					
S1458	n-tex	Conc	Normal	3.4	8.2×10^{10}	1.8×10^{11}	1398	6×10^{-18}	7×10^{-17}
S1460	n-tex	Conc	Half	6.8	3.1×10^{11}	1.5×10^{11}	158	6×10^{-18}	7×10^{-17}
S1466	n-tex	Conc	Double	1.7	3.3×10^{11}	4.0×10^{11}	1023	6×10^{-18}	7×10^{-17}
S1467	n-tex	Conc	Double	0.8	6.8×10^{11}	6.0×10^{11}	777	6×10^{-18}	7×10^{-17}
Reaction time series									
			Time (min)						
S1381	n-tex	Time	30		3.6×10^{11}	4.0×10^{11}	1030	5×10^{-18}	6×10^{-17}
S1382	n-tex	Time	60		2.8×10^{11}	3.5×10^{11}	1046	5×10^{-18}	6×10^{-17}
S1384	n-tex	Time	15		3.2×10^{11}	3.8×10^{11}	1151	5×10^{-18}	6×10^{-17}
S1387	n-tex	Time	210		2.4×10^{11}	3.0×10^{11}	1141	5×10^{-18}	6×10^{-17}
S1383	n-tex	Time	120		3.7×10^{11}	3.8×10^{11}	989	5×10^{-18}	6×10^{-17}

An interesting trend from this model is a linear relationship between D_{it} and Q_f across all samples. [Fig. 4.14] Previous results showed an inverse non-linear relationship. [34] The cause of this difference is not known. There is one particular outlier with S1460 (due to a very different lifetime curve than the other samples) but this model requires further investigation of D_{it} and Q_f by experimental methods to confirm and derive any model for this relationship.

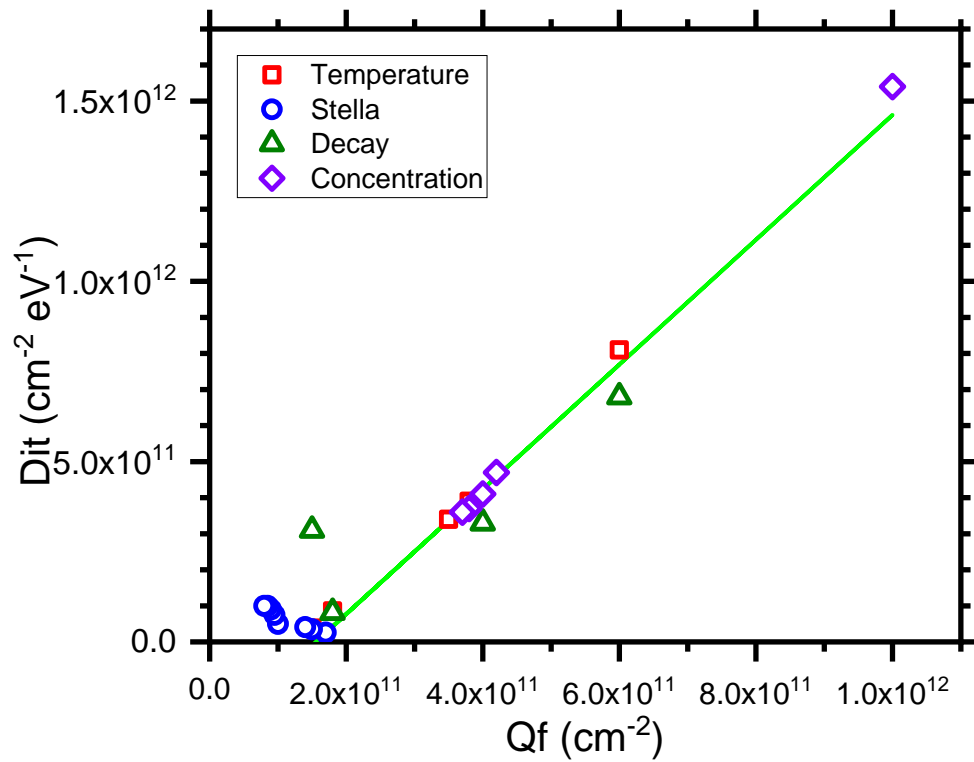


Figure 4.14 Relationship between D_{it} and Q_f .

Chapter 5

CONCLUSION

A series of sulfur passivation experiments have been performed on n- and p-type Cz Si wafers that suggest several trends in the performance and structure of said passivation. S passivation can be performed at a much lower temperature than SiO₂ (550°C as opposed to 900°C), to achieve similar surface passivation quality (SRV <3 cm/s). Reaction time can be modified to increase the stability of the S passivation, and it can be further improved with the application of an a-SiN_x layer. This passivation stack is shown to stabilize passivation quality even after thermal simulation firing, necessary for contact formation. A high total gas flow rate in atmospheric pressure H₂S reaction process can significantly improve SRV. p-type wafers show a lower lifetime than n-type wafers, in part due to poorer bulk quality of the p-type wafers used in our study. There has also been progress in the cleaning and passivation of dopant diffused wafers, where n-n⁺ wafers have proved much easier to passivate than n-p⁺ wafers. Performance with an a-SiN_x capping layer is comparable to other current techniques, with the best SRV of S passivation being <2 cm/s, competitive with state-of-the-art SiO₂ passivation (< 1 cm/s) and a-Si:H (<4 cm/s).

Modelling has been performed to analyze these results in a more objective manner, revealing an unexplained correlation between D_{it} and Q_f. Further research in this regard could include a more in-depth exploration of lifetime modelling, with

experimentally confirmed D_{it} and Q_f . The experimental techniques performed here have not considerably examined the effects of the S passivation on the bulk of the wafer, which may provide an answer for the modelling behavior. Another test that could compliment this modelling is a C-V test that can give more accurate guesses of D_{it} and Q_f . By basing these numbers off of experimental data, it can reduce the number of variables that the model has to fit to, as well as hint at refinements to the recombination model itself.

BIBLIOGRAPHY

- [1] E. Kaxiras, “Semiconductor-surface restoration by valence-mending adsorbates: Application to Si(100):Sand Si(100):Se,” *Phys. Rev. B*, vol. 43, no. 8, pp. 6824–6827, 1991.
- [2] H. Y. Liu, U. K. Das, and R. W. Birkmire, “Surface defect passivation and reaction of c-Si in H₂S,” *Langmuir*, vol. 33, no. 51, pp. 14580–14586, 2017, doi: 10.1021/acs.langmuir.7b03520.
- [3] A. Chodos, “April 25, 1954: Bell Labs Demonstrates the First Practical Silicon Solar Cell,” *APS News*, vol. 18, no. 4, 2009.
- [4] “Solar Industry Data Overview,” *Solar Energy Industries Association*, 2020. [Online]. Available: <https://www.seia.org/solar-industry-research-data>. [Accessed: 09-Nov-2020].
- [5] C. Honsberg and S. Bowden, “PVEducation.org,” *Solar Power Lab at Arizona State University*, 2019. [Online]. Available: <https://www.pveducation.org/pvcdrom/welcome-to-pvcdrom>. [Accessed: 08-Aug-2020].
- [6] M. Y. Ali and M. Tao, “Effect of sulfur passivation of silicon (100) on Schottky barrier height: Surface states versus surface dipole,” *J. Appl. Phys.*, vol. 101, no. 10, pp. 1–5, 2007, doi: 10.1063/1.2733611.
- [7] B. Shu, U. Das, J. Appel, B. McCandless, S. Hegedus, and R. Birkmire,

- “Alternative approaches for low temperature front surface passivation of interdigitated back contact silicon heterojunction solar cell,” *Conf. Rec. IEEE Photovolt. Spec. Conf.*, pp. 3223–3228, 2010, doi: 10.1109/PVSC.2010.5616755.
- [8] Z. Shu, U. K. Das, J. Allen, R. W. Birkmire, and S. Hegedus, “Experimental and simulated analysis of front versus all- back-contact silicon heterojunction solar cells: effect of interface and doped a-Si:H layer defects,” *Prog. Photovoltaics Res. Appl.*, vol. 23, pp. 78–93, 2015, doi: 10.1002/pip.2400.
- [9] M. Green, *Solar Cells*. Englewood Cliffs, N.J.: Prentice-Hall, 1982.
- [10] H.-Y. Liu, “Silicon defect passivation by H₂S reaction and patterning process of interdigitated back contact silicon heterojunction (IBC-SHJ) solar cell,” Ph.D dissertation, College of Eng., University of Delaware, DE, 2018.
- [11] R. S. Bonilla, B. Hoex, P. Hamer, and P. R. Wilshaw, “Dielectric surface passivation for silicon solar cells: A review,” *Phys. Status Solidi Appl. Mater. Sci.*, vol. 214, no. 7, 2017, doi: 10.1002/pssa.201700293.
- [12] M. Kuhn, “A quasi-static technique for MOS C-V and surface state measurements,” *Solid State Electron.*, vol. 13, no. 6, pp. 873–885, 1970, doi: 10.1016/0038-1101(70)90073-0.
- [13] N. Khedher *et al.*, “Gettering impurities from crystalline silicon by phosphorus diffusion using a porous silicon layer,” *Sol. Energy Mater. Sol. Cells*, vol. 87, no. 1–4, pp. 605–611, 2005, doi: 10.1016/j.solmat.2004.09.017.
- [14] V. D. Mihailetchi, Y. Komatsu, and L. J. Geerligs, “Nitric acid pretreatment for the passivation of boron emitters for n -type base silicon solar cells,” *Appl. Phys.*

- Lett.*, vol. 92, no. 6, pp. 14–17, 2008, doi: 10.1063/1.2870202.
- [15] X. Sun *et al.*, “Borosiloxane boron diffusion for p-emitter formation on n-type silicon wafers,” *J. Mater. Sci. Mater. Electron.*, vol. 28, no. 16, pp. 11563–11568, 2017, doi: 10.1007/s10854-017-6956-9.
- [16] B. Hoex, J. Schmidt, R. Bock, P. P. Altermatt, M. C. M. Van De Sanden, and W. M. M. Kessels, “Excellent passivation of highly doped p -type Si surfaces by the negative-charge-dielectric Al₂ O₃,” *Appl. Phys. Lett.*, vol. 91, no. 11, pp. 1–4, 2007, doi: 10.1063/1.2784168.
- [17] J. Schmidt, R. Peibst, and R. Brendel, “Surface passivation of crystalline silicon solar cells: Present and future,” *Sol. Energy Mater. Sol. Cells*, vol. 187, no. January, pp. 39–54, 2018, doi: 10.1016/j.solmat.2018.06.047.
- [18] T. L. Christiansen, O. Hansen, J. A. Jensen, and E. V. Thomsen, “Thermal Oxidation of Structured Silicon Dioxide,” *ECS J. Solid State Sci. Technol.*, vol. 3, no. 5, pp. N63–N68, 2014, doi: 10.1149/2.003405jss.
- [19] S. MacK *et al.*, “Silicon surface passivation by thin thermal oxide/PECVD layer stack systems,” *IEEE J. Photovoltaics*, vol. 1, no. 2, pp. 135–145, 2011, doi: 10.1109/JPHOTOV.2011.2173299.
- [20] G. Dingemans, M. C. M. Van De Sanden, and W. M. M. Kessels, “Excellent Si surface passivation by low temperature SiO₂ using an ultrathin Al₂O₃ capping film,” *Phys. Status Solidi - Rapid Res. Lett.*, vol. 5, no. 1, pp. 22–24, 2011, doi: 10.1002/pssr.201004378.
- [21] C. Battaglia, A. Cuevas, and S. De Wolf, “High-efficiency crystalline silicon solar

- cells: Status and perspectives,” *Energy Environ. Sci.*, vol. 9, no. 5, pp. 1552–1576, 2016, doi: 10.1039/c5ee03380b.
- [22] J. R. Elmiger and M. Kunst, “Investigation of charge carrier injection in silicon nitride/silicon junctions,” *Appl. Phys. Lett.*, vol. 69, no. 4, pp. 517–519, 1996, doi: 10.1063/1.117772.
- [23] S. Duttagupta, F. Ma, B. Hoex, T. Mueller, and A. G. Aberle, “Optimised antireflection coatings using silicon nitride on textured silicon surfaces based on measurements and multidimensional modelling,” *Energy Procedia*, vol. 15, no. 2011, pp. 78–83, 2012, doi: 10.1016/j.egypro.2012.02.009.
- [24] J. Schmidt, A. Merkle, R. Brendel, B. Hoex, M. C. M. van de Sanden, and W. M. M. Kessels, “Surface passivation of high-efficiency silicon solar cells,” *Prog. Photovolt Res. Appl.*, vol. 16, pp. 461–466, 2008, doi: 10.1002/pip.823.
- [25] R. Kotipalli, B. Vermang, J. Joel, R. Rajkumar, M. Edoff, and D. Flandre, “Investigating the electronic properties of Al₂O₃/Cu(In,Ga)Se₂ interface,” *AIP Adv.*, vol. 5, no. 10, 2015, doi: 10.1063/1.4932512.
- [26] G. Dingemans and W. M. M. Kessels, “Status and prospects of Al₂O₃-based surface passivation schemes for silicon solar cells,” *J. Vac. Sci. Technol. A Vacuum, Surfaces, Film.*, vol. 30, no. 4, p. 040802, 2012, doi: 10.1116/1.4728205.
- [27] M. Tanaka *et al.*, “Development of New a-Si/c-Si Heterojunction Solar Cells: ACJ-HIT (Artificially Constructed Junction-Heterojunction with Intrinsic Thin-Layer),” *Jpn. J. Appl. Phys.*, vol. 31, p. 3158, 1992.
- [28] S. DeWolf, A. Descoedres, Z. C. Holman, and C. Ballif, “High-efficiency silicon

- heterojunction solar cells: A review,” *Green*, vol. 2, no. 1, pp. 7–24, 2012, doi: 10.1515/green-2011-0018.
- [29] B. Shu, U. Das, J. Appel, B. McCandless, S. Hegedus, and R. Birkmire, “Low temperature front surface passivation of interdigitated back contact silicon heterojunction solar cell,” *Conf. Rec. IEEE Photovolt. Spec. Conf.*, pp. 1316–1320, 2009, doi: 10.1109/PVSC.2010.5616755.
- [30] M. Stutzmann, W. B. Jackson, and C. C. Tsai, “Light-induced metastable defects in hydrogenated amorphous silicon: A systematic study,” *Phys. Rev. B*, vol. 32, no. 1, pp. 23–47, 1985, doi: 10.1103/PhysRevB.32.23.
- [31] U. K. Das, M. Z. Burrows, M. Lu, S. Bowden, and R. W. Birkmire, “Surface passivation and heterojunction cells on Si (100) and (111) wafers using dc and rf plasma deposited Si:H thin films,” *Appl. Phys. Lett.*, vol. 92, no. 6, pp. 1–3, 2008, doi: 10.1063/1.2857465.
- [32] P. A. G. O'Hare, “Thermochemistry of silicon-containing materials *,” *Pure Appl. Chem.*, vol. 71, no. 7, pp. 1243–1248, 1999.
- [33] A. Haas, “The Chemistry of Silicon-Sulfur Compounds,” *Angew. Chem. internat. Edit.*, vol. 819, no. 1, pp. 1014–1023, 1965.
- [34] U. Das, S. Jafari, L. Zhang, H. Y. Liu, R. Birkmire, and S. Hegedus, “Si surface passivation by sulfur and reduction of interface defect recombination,” *2018 IEEE 7th World Conf. Photovolt. Energy Conversion, WCPEC 2018 - A Jt. Conf. 45th IEEE PVSC, 28th PVSEC 34th EU PVSEC*, no. 100, pp. 3076–3079, 2018, doi: 10.1109/PVSC.2018.8547951.

- [35] “Wet-Chemical Etching and Cleaning of Silicon,” *Virginia Semiconductor Inc.*, 2003. [Online]. Available: https://www.virginiasemi.com/?cont_uid=54. [Accessed: 11-Nov-2020].
- [36] B. Chhabra, S. Bowden, R. L. Opila, and C. B. Honsberg, “High effective minority carrier lifetime on silicon substrates using quinhydrone-methanol passivation,” *Appl. Phys. Lett.*, vol. 96, no. 6, pp. 1–4, 2010, doi: 10.1063/1.3309595.
- [37] R. A. Sinton and A. Cuevas, “Contactless determination of current-voltage characteristics and minority-carrier lifetimes in semiconductors from quasi-steady-state photoconductance data,” *Appl. Phys. Lett.*, vol. 69, no. 17, pp. 2510–2512, 1996, doi: 10.1063/1.117723.
- [38] R. Sinton, A. Cuevas, and M. Stuckings, “Quasi-steady-state Photoconductance, a new method for solar cell material and device characterization,” *IEEE 25th PVSC*, pp. 457–460, 1996.
- [39] F. M. Smits, “Measurement of Sheet Resistivities with the Four-Point Probe,” *Bell Syst. Tech. J.*, vol. 37, no. 3, pp. 711–718, 1958, doi: 10.1002/j.1538-7305.1958.tb03883.x.
- [40] M. Schmidt *et al.*, “Physical and Technological Aspects of a-Si:H/c-Si Hetero-Junction Solar Cells,” in *Photovoltaic Energy Conversion, Conference Record of the 2006 IEEE 4th World Conference on*, 2006, doi: 10.1109/WCPEC.2006.279722.
- [41] F. C. Chiu, “Surface state capture cross-section at the interface between silicon and hafnium oxide,” *Adv. Mater. Sci. Eng.*, vol. 2013, 2013, doi:

10.1155/2013/950439.